Marine Geology 378 (2016) 213–229

Contents lists available at ScienceDirect

Marine Geology

journal homepage: www.elsevier.com/locate/margo

Sedimentary processes determining the modern carbonate periplatform drift of Little Bahama Bank

Ludivine Chabaud [a,*], Emmanuelle Ducassou [a], Elsa Tournadour [a], Thierry Mulder [a], John J.G. Reijmer [b], Gilles Conesa [c], Jacques Giraudeau [a], Vincent Hanquiez [a], Jean Borgomano [c], Lauren Ross [a]

[a] Université de Bordeaux, UMR CNRS 5805 EPOC, Allée Geoffroy Saint-Hilaire, 33615, Pessac CEDEX, France
[b] University Amsterdam, Faculty of Earth and Life Sciences, Sedimentology and Marine Geology Group, De Boelelaan 1085, 1081 HV Amsterdam, The Netherlands
[c] Aix-Marseille Université, CEREGE UM 34, 3, Pl. Victor Hugo, 13331 Marseille Cedex 3, France

ARTICLE INFO

Article history:
Received 13 May 2015
Received in revised form 6 November 2015
Accepted 15 November 2015
Available online 21 November 2015

Keywords:
Modern carbonate contourites
Periplatform drift
Bahamas
Stratigraphy
Sedimentary records
Quaternary

ABSTRACT

This paper presents an analysis of the combined influence of along-slope sediment transport and off-bank sediment export from the Little Bahama Bank (LBB) to the periplatform sediment wedge of the northwestern part of the slope over the last 424 ka. The LBB northwestern slope is divided in (i) a plateau-like structure (margin) at ~40 m water depth over at least 4 km parallel to the edge of the LBB; (ii) the uppermost slope with a mean slope angle of ~1.15° from 40 to 300 m water depth; (iii) the upper slope with slope angle of ~0.7 from 300 to 650 m water depth, (iv) the middle slope with slope angle of ~1.2, from 650 to 800 m water depth, and (v) the lower slope with slope angle of <~0.5, from 800 to 900 m water depth.

The uppermost slope, the upper slope, and the middle slope of the northwestern LBB were characterized by periplatform oozes that became more diluted with pelagic sediment toward the distal part of the slope. This sediment distribution of the northwestern LBB slope varied significantly over times according to the flooded surface of the LBB. The major flooding periods are related to the highest Relative Sea Level (RSL) (>−6 m) that occurred during interglacial periods, the highest sedimentation rates (10–30 cm/ka) and the finest sediment facies were found on the slope. During interglacial periods when RSL < −6 m, LBB was emerged but bank margins were still flooded and correspond to intermediate sedimentation rates (a few to 10 cm/ka) on the slope. Finally, during glacial periods (RSL < −90 m), LBB was emerged (including its margins), sedimentation rates on the slope dropped to a few mm/ka associated to coarser sediment facies.

Off-bank-transported sediment is the main sediment supply during sea-level highstands, occurring preferentially during three major periods of LBB flooding over the last 424 ka: marine isotopic stages 1, 5e and 11. During sea-level lowstands, shallow carbonate production was very low but could develop over a 4 km-wide plateau-like structure when RSL was above −40 m. The regional Antilles Current affected the sea floor along the northwestern LBB slope and influenced coral mound distribution as well as sediment facies and sequences along the upper and middle slopes (300–800 m). During glacial periods, the stronger influence of the Antilles Current upon the along-slope sedimentation promoted diagenesis via the development of indurated nodules in the upper slope (~400 m water depth). It also encouraged bi-gradational sequences showing a coarsening-up unit followed by a fining-up unit along the middle slope (~800 m water depth) that is thoroughly bioturbated. The characteristics of these contourite sequences were similar to those described in siliciclastic environments, but in contrast were condensed with low sedimentation rates over long (glacial) periods.

1. Introduction

Contourite drifts were first defined as large accumulations of sediment deposited at water depths exceeding 500 m by deep water bottom-currents circulating over the sea floor related to thermohaline circulation (Heezen et al., 1966; Heezen and Hollister, 1971; Hollister and Heezen, 1972; Faugères and Stow, 1993). Recently, the term "contourite drift" was also applied to deposits along continental margins built by intermediate (Van Rooij et al., 2010; Rebesco et al., 2013) or shallow (e.g. Vandorpe et al., 2011) water masses. Contourite drift morphology ranges from small patch drifts (<100 km^2) to giant elongate drifts (>100,000 km^2) (for a complete review see Faugères et al., 1999; Rebesco and Camerlenghi, 2008; Faugères and Mulder, 2011; Rebesco et al., 2014). The relatively continuous accumulation rates of contourite drifts (Knutz, 2008) provide a record of paleoenvironmental changes throughout time (Hernández-Molina et al., 2003; Llave et al.,

* Corresponding author.
E-mail address: ludivine.chabaud.fr@gmail.com (L. Chabaud).

http://dx.doi.org/10.1016/j.margeo.2015.11.006
0025-3227/

2006; Voelker et al., 2006; Wilson, 2012, 2013; Toucanne et al., 2012; Mulder et al., 2013; Vandorpe et al., 2014).

Contourite deposits are widely documented in the literature (Stow and Holbrook, 1984; Faugères et al., 1999; Faugères and Stow, 2008; Stow et al., 2002, 2008). However, only few studies have highlighted the importance of contour-currents along carbonate slopes (Neumann and Ball, 1970; Correa et al., 2012; Betzler et al., 2013; Murdmaa et al., in this issue). Five modern carbonate contourite drifts can be found in the Bahamas: the Pourtales Drift, the Santaren Drift, the Cay Sal Drift, the Great Bahama Bank (GBB) Drift, and the Little Bahama Bank (LBB) Drift (Mullins et al., 1980; Anselmetti et al., 2000; Bergman, 2005; Bergman et al., 2010). The term "periplatform drift" was recently introduced (Betzler et al., 2014) to refer to a carbonate slope wedge that is under the influence of ocean currents. Such periplatform drifts are very specific compared to other drifts as the main sediment input result from off-bank transport of the carbonate platform located nearby. The classical contourite facies is characterized by a bioturbated coarsening-up unit ranging from the muddy facies to silty/sandy facies, followed by a bioturbated fining-up unit ending back with muddy facies. Such a facies succession described from the Faro Drift in the Gulf of Cádiz reflects the intensification and reduction of current velocities (Gonthier et al., 1984; Faugères et al., 1984). The term "contourite" represents one bigradational sedimentary sequence, and the term "contourite drift" refers to the staking of contourites forming the sedimentary body.

In carbonate environments, remarkable changes in sedimentation rates have been observed along slopes with a high (low) accumulation of sediment during interglacial (glacial) periods (firstly documented by Kier and Pilkey, 1971; Lynts et al., 1973; Mullins et al., 1980; Mullins, 1983; Droxler et al., 1983). During sea-level highstands, the complete submersion of the shallow-water carbonate bank, water depth <6 m, is allowed for the abundant production of fine-grained aragonite particles on the LBB (Neumann and Land, 1975). Production of sediment on the carbonate bank is sharply reduced when the bank top is partially or totally emerged during lowstands. Episodic sedimentation due to sea-level fluctuations between glacial and interglacial periods is explained by the "highstand shedding" model (Droxler and Schlager, 1985; Schlager et al., 1994), which is highlighted in numerous studies (Mullins et al., 1980; Boardman and Neumann, 1984; Boardman et al., 1986; Reijmer et al., 1988; Wilber et al., 1990; Rendle and Reijmer, 2002).

This study analyzed the spatial and temporal variability of sedimentation on the LBB Drift (~400 and ~800 m water depth). In addition, it aimed to highlight sedimentary processes at varying distances from the bank over the last 424 ka (highstand vs lowstand). A multi-proxy approach based on bio- and isotopic stratigraphy and sedimentary analyses of marine cores was combined with geometrical analyses of geophysical data. The aim of this paper is to explain the growth of this contourite drift and discuss the use of the term periplatform drift.

2. Present-day environmental setting

2.1. Geological, climatic and oceanographic contexts

The Bahamian archipelago is composed by several shallow-water carbonate banks (Fig. 1) and has been considered tectonically stable since the middle Tertiary (Masaferro and Eberli, 1999). It forms an isolated platform with limited wind-derived siliciclastic supply and represents (in maximum) less than 3.4% of the platform sedimentation (Traverse and Ginsburg, 1966; Swart et al., 2014). The Bahamas is nowadays considered as a fairly pure carbonate sedimentation environment. The climate of the northern Bahamas is subtropical to temperate (Roth and Reijmer, 2004) with easterly trade winds (from NE, E, and SE) most of the year and cold northwesterly winds occurring during winter (Sealey, 1994). Wave energy flux is higher on the northern margin of the LBB (windward) than the southern and western margins of LBB (leeward) (Hine and Neumann, 1977; Hine et al., 1981a, 1981b). Oceanic circulation patterns in the northern Bahamas are complex. However, it is broadly accepted that the Antilles Current flows to the Northeast along the Bahama Escarpment and to the North of LBB (Rowe et al., 2015), where it merges with the Florida Current to form the Gulf Stream (Neumann and Pierson, 1966; Rowe et al., 2015). The only known current pattern described north of Little Bahama Bank suggests stronger currents at 400 m water depth than 50 m water depth (Fig. 2, Johns, 2011), which is in agreement with highest velocities located in 400 m water depth to the east of LBB (Lee et al., 1990). Measurements of the Antilles Current taken on the eastern part of the LBB northern slope recorded flow velocities at 750 m water depth ranging from 0.2 to 0.8 m/s directed northwest (Costin, 1968). In the same area, a reversal of bottom current across the east–west axis was recorded at 1040 m water depth but without quantification of the velocities (Gallagher, 1968). It has been suggested that the Antilles Current is not a steady flow but behaves as an eddy field along the Bahamian Archipelago (Gallagher, 1968; Ingham, 1974; Gunn and Watt, 1982; Lee et al., 1996). The Florida Current stretches northward from the Straits of Florida to Cape Hatteras (Rowe et al., 2015) with a discharge of 32.1 ± 3.3 Sv (Baringer and Larsen, 2001; Rousset and Beal, 2014). The surface currents are strongest on the western side of the straits, above the continental slope off Miami, with maximum velocities exceeding 1.5 to 2 m/s (Brooks and Niiler, 1977). Under this surface current (457 to 825 m water depth), southward-flowing countercurrents are found with average velocities of 0.18 m/s, and maximum velocities of 0.6 m/s (Neumann and Ball, 1970; Correa et al., 2012). Bottom currents along the eastern side of the Bahamas flow to the north at velocities reaching 0.5 m/s at 305 m water depth (Neumann and Ball, 1970; Neumann et al., 1977).

2.2. Geometry of the LBB Drift

In the Bahamas, the LBB Drift is a modern carbonate contourite drift that settled along the western side of the northern LBB slope (Mullins et al., 1980). The LBB Drift extends over 100 km (with a slope inclination around 1°) and a maximum width of 60 km (Mullins et al., 1980). According to the classification of Faugères et al. (1999), the LBB Drift corresponds to a plastered drift influenced by down-slope processes (Tournadour et al., 2015). The LBB Drift began approximately during the Miocene or Pliocene (Unit F in Fig. 3, Tournadour et al., 2015). A huge mass transport complex (Tournadour et al., 2015) affected the upper slope of the LBB Drift and the mass transport deposits formed a compressional area on the frontal edge (light blue of Unit F in Fig. 3) which may have been affected by a major erosional event (top of Unit F in Fig. 3). A major growth phase occurred during the entire Quaternary (Unit G, in Fig. 3), which is the main focus of this study.

LBB Drift deposits consist of a mixture of planktonic and pelagic microfauna living in the water column and sediments derived from the adjacent LBB (Mullins et al., 1980; Lantzsch et al., 2007), hence a typical "periplatform ooze" (Schlager and James, 1978). Lantzsch et al. (2007) showed, from sediment cores MD99-2202 (Figs. 1, 4A), fine-grained sediment with a high aragonite content during interglacial periods, and cemented coarser sediment with a high-Mg calcite content during glacial periods. Hardgrounds are present on the sea floor at approximately 600 to 700 m water depth in the Straits of Florida and, along the base of LBB (Neumann and Ball, 1970; Neumann et al., 1977; Mullins and Neumann, 1979). These can be explained by winnowing related to currents affecting the sea floor (Wilber, 1976), and the diagenetic potential of periplatform oozes (Heath and Mullins, 1984). Both mechanisms vary in intensity with distance from the edge of the bank (Mullins et al., 1985). Additionally, elongated carbonate mounds (lithoherms) have been observed on the western margin of LBB in the Straits of Florida (Neumann et al., 1977; Messing et al., 1990). These mounds were thought to be mainly controlled by currents providing nutrients, and by sea floor topography (Correa et al., 2012). ROV observations revealed that they were occasionally just carbonate blocks with a coral cover (Hebbeln et al., 2012). However, east of the study area deep carbonate coral mounds (bioherms) have been reported at depths

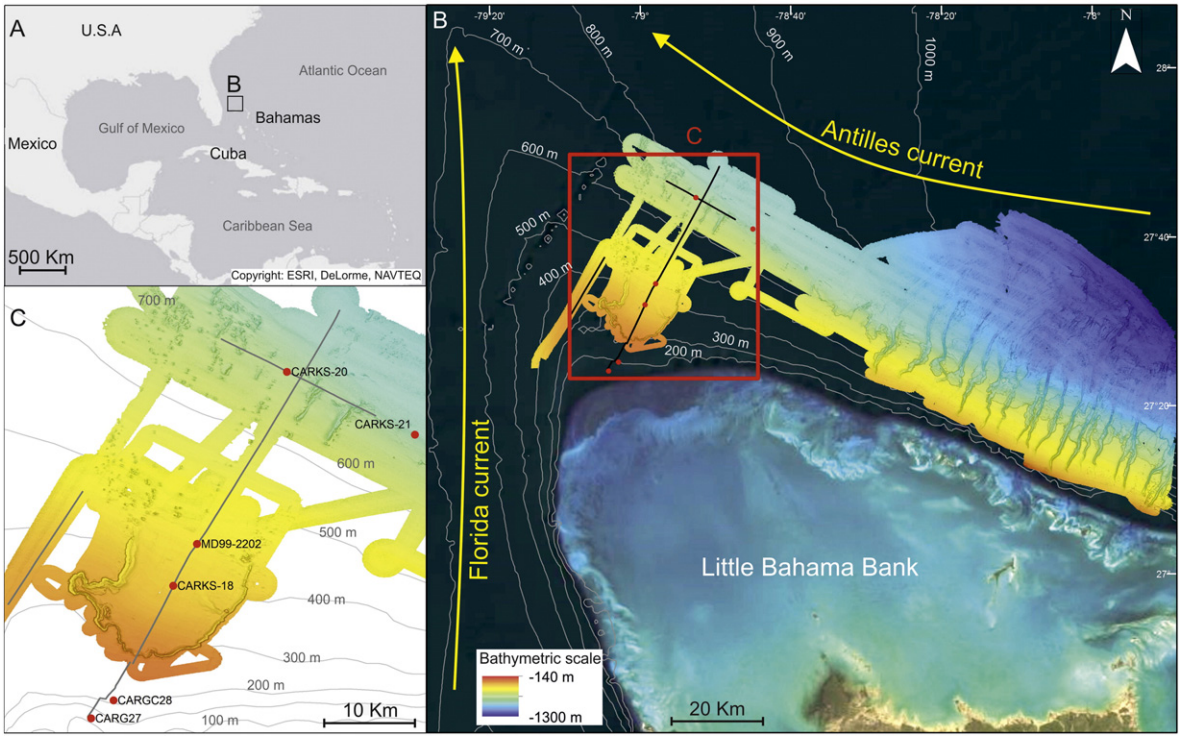

Fig. 1. A) Location map study area, north of the Bahamas; B) Bathymetric map of carbonate slope located north of LBB (Leg 2 — CARAMBAR cruise). Yellow arrows indicate main ocean currents. Red points indicate location of marines cores used in this study. Purple dots and line indicate the location of the sound velocity profiles (CARAMBAR 1.5 cruise); C) Zoom on the LBB Drift. Names of cores are added. Isobaths are drawn after the General Bathymetric Chart of the Oceans (GEBCO, 2014) data set.

of 1000–1300 m water depth with sediment starved ripples in intermound area (Mullins et al., 1981; Reed, 2002).

3. Materials and methods

3.1. Very high-resolution (VHR) seismic data and sedimentary cores

The dataset used in this study was collected in the LBB Drift along the northwest end of the LBB (Fig. 1) during the Carambar Cruise (2010) aboard the R.V. *Le Suroît* (Mulder et al., 2012a, 2012b) and Carambar 1.5 Cruise (2014) on the R.V. *F.G. Walton Smith*. The MD99-2202 core (Table 1) obtained on the LBB Drift in 1999 with the RV Marion Dufresne was added to the dataset (Lantzsch et al., 2007).

All cores (Table 1) were recovered on the westernmost side of the northern slope off LBB and penetrated to Unit G, which fills the depression of the mass transport complex (Fig. 2). Cores CARKS-18, CARKS-20 and CARKS-21 were collected using a Kullenberg piston corer ca 15, 37 and 30 km from the bank edge (Fig. 1). Core CARG-28 was collected

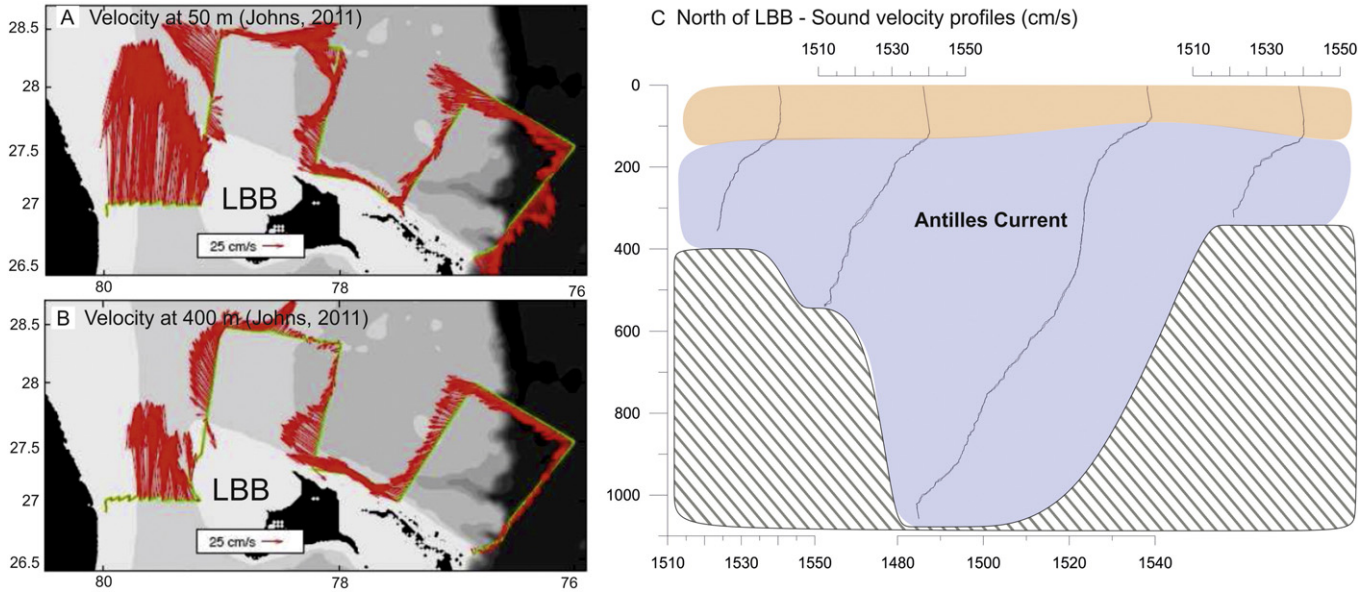

Fig. 2. : Currents patterns A) at 50 m and B) at 400 m obtained during the shipboard ADCP survey north of Little Bahama Bank, and from the Florida Current section at 27° N (Johns, 2011). C) Sound velocity profiles located on the study area north of LBB (purple dot and lines on Fig. 1).

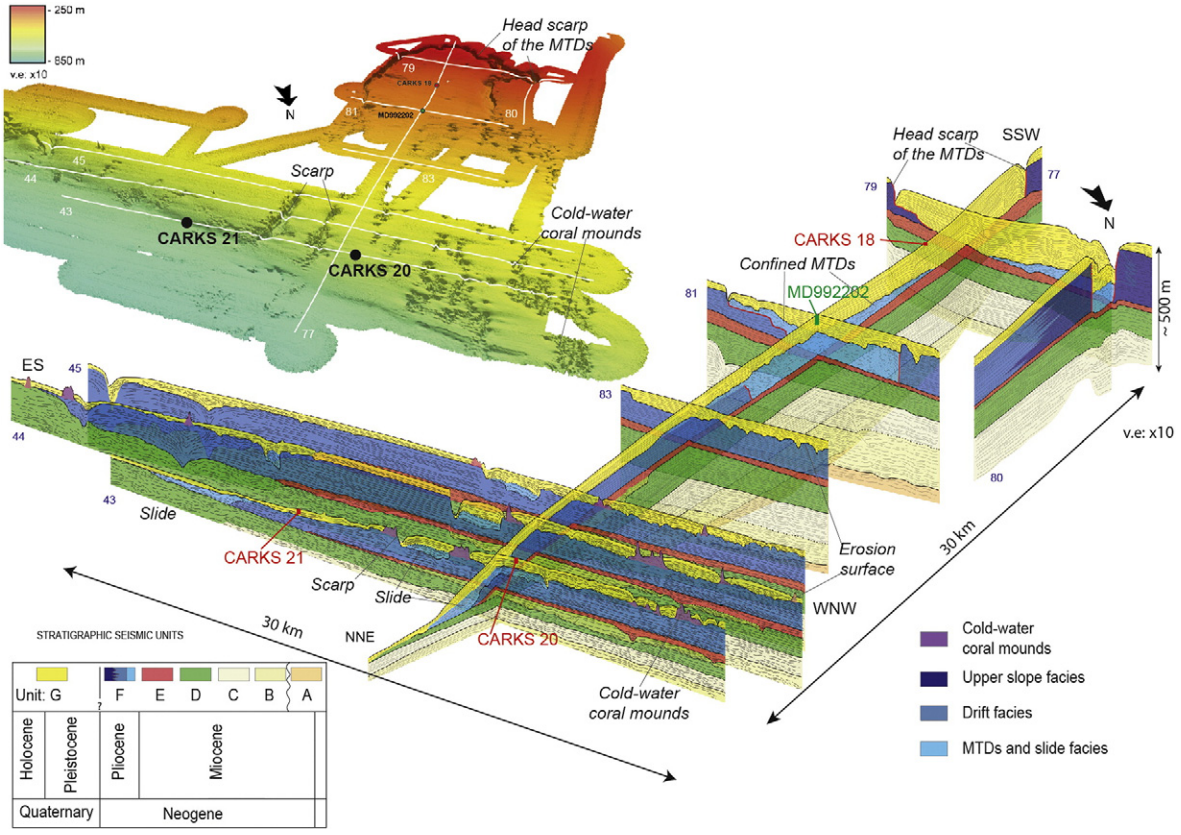

Fig. 3. 3D assemblages view of the seismic interpretation of the LBB Drift (Tournadour et al., 2015). The LBB Drift structured the northwest corner of LBB slope by a hemiconical body with a downslope termination at 800 m water depth.

using a gravity core ca 4 km from the bank edge (Fig. 1). CARG-27 was collected using a Van Veen grab ca 2 km from the bank edge (Fig. 1).

Approximately 600 km of VHR seismic lines were collected in the LBB Drift from a sub-bottom profiler (Chirp mode). The litho-seismic correlation of the cores (CARKS-18, 20 and 21) was made with an average velocity of 1700 m/s (Sheridan et al., 1966; Harwood and Towers, 1988). It should be noted that the accuracy of VHR seismic lines is ~0.5 ms so ~0.4 m on core sections.

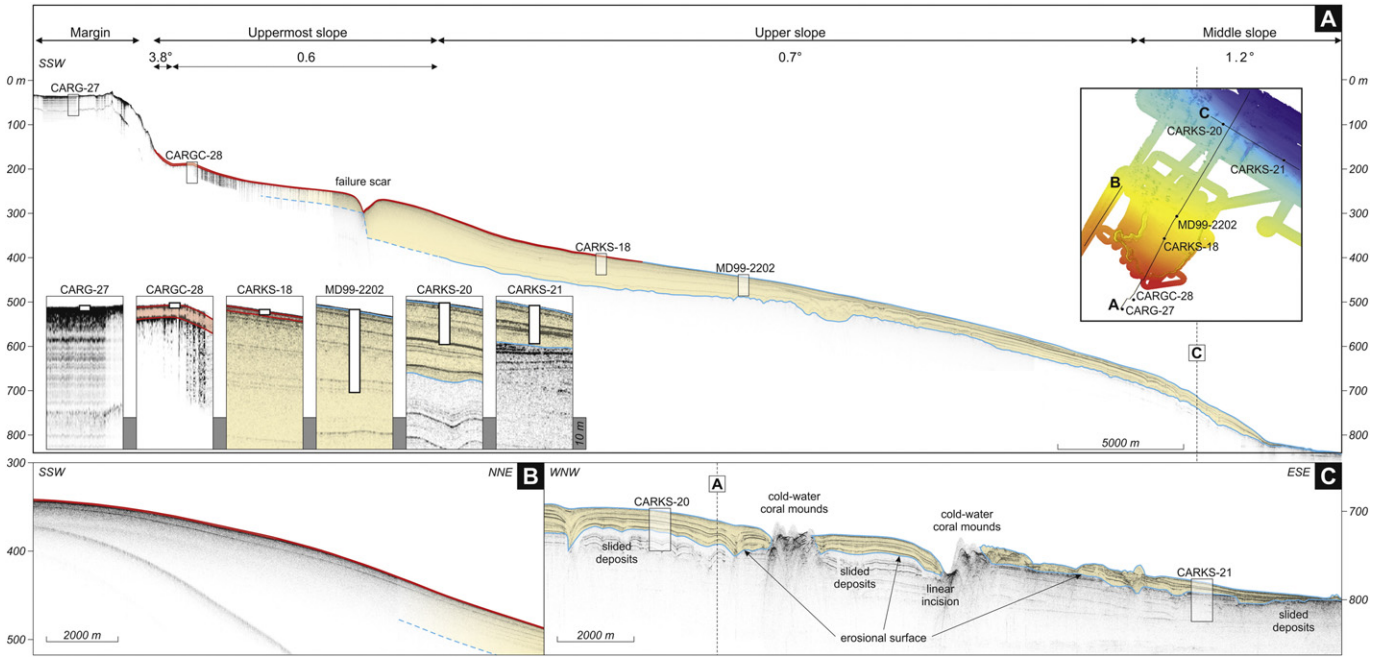

Fig. 4. A) Overview of VHR seismic lines 143, 224, 225 and 229 from CARAMBAR cruise and lines 110, 111 and 112 from CARAMBAR 1.5 and an enlargement of core site locations. The margin and the name and angles of the different units of the slope are indicated; B) VHR seismic line 229 showing the slope morphology and internal sediment wedge structures; C) VHR seismic line 143 with various details. Yellow unit corresponds to Unit G described in Tournadour et al. (2015).

Table 1
Information of the studied cores including name: the coring method, the length of recovery (cm), the water depth (m water depth), the latitude and the longitude.

Name	Coring method	Length of recovery (cm)	Water depth (m)	Latitude	Longitude
CARKS-18	Kullenberg piston corer	100	404	27°31.9746′ N	78°59.34813′ W
CARKS-20	Kullenberg piston corer	1311	714.2	27°44.66326′ N	78°52.59793′ W
CARKS-21	Kullenberg piston corer	1195	798.8	27°40.9360′ N	78°45.0075′ W
CARGC-28	Gravity core	~4	191	27°25.179′° N	79°02.881′° W
CARG-27	Van Veen grab	7 (indurated block)	68	27°24.116′° N	79°04.213′° W
MD99-2202	Calypso Giant Piston Corer	26	460	27°34.45′ N	78°57.93′ W

Sound Velocity profiles were performed along the water column using a Minos X vertical profiler at 6 different locations (Fig. 1) in order to identify water masses (Fig. 2).

3.2. Sedimentological analyses

All sedimentological analyses were performed in the CNRS-EPOC and RAMAT-CRP2A (SEM images) research laboratories of the University of Bordeaux. Only a few centimeters of sediment were recovered from CARG-28 and an indurated block was recovered from CARG-27, which prevented sedimentological analyses. The sedimentological analyses of the CARKS-18, CARKS-20, and CARKS-21 cores consisted of a visual description, photography, and sediment color measurement using a spectrophotocolorimeter Minolta CM2600D.

X-ray analyses were performed using the SCOPIX X-ray image-processing tool (Migeon et al., 1999). Downcore patterns of strontium and calcium content were measured every cm in CARKS-18, CARKS-20 and CARKS-21 with an Avaatech XRF scanner (10 kV, 400 μA, 10 s, and 30 kV 2000 μA, 15 s). Strontium counts were normalized by calcium counts in order to correct for potential biases associated with the measuring method (mainly variations in water content and grain-size). Grain size was measured using a Malvern Mastersizer S laser diffractometer with the Fraunhofer method. The 50th centile (D50 or median) and modal distribution of the sediment were used and shown in the core analysis figures. Four thin sections were collected in core CARKS-21 and in CARKS-18 and the preparation technique used for these sections followed the protocol described in http://www.epoc.u-bordeaux.fr/index.php?lang=fr&page=eq_sedimentologie7 (Zaragosi et al., 2006). Thin section images were then acquired using an automated LEICA DM6000 B Digital Microscope at ×25 magnifications (Zaragosi et al., 2006). In addition, high-resolution images were made using a Scanning Electron Microscopy (SEM) JEOL 6460 LV. Samples of bulk sediment were dried and coated with gold for five minutes to ensure conductivity was at an adequate level to use the high vacuum mode.

3.3. Biostratigraphical and isotopic analyses

Five AMS ^{14}C dates were performed at the Laboratoire du Carbone 14 (Saclay, France) on monospecific samples of the planktonic foraminifera *Globigerinoides ruber* var. *alba*: two on core CARKS-20 over the top 60 cm and three on core CARKS-21 over the top 140 cm.

δ^{18}O measurements were carried out at CNRS-EPOC research laboratory (University of Bordeaux) on ~10 tests of the planktonic foraminifer species *G. ruber* var. *alba* collected from the 200–250 μm sediment fraction every 10 cm on CARKS-21 using an Optima Micromass mass spectrometer. Data were reported as δ^{18}O versus Pee Dee Belemnite standard (PDB) after calibration with National Bureau of Standards (NBS) 19 (Coplen, 1988; Hut, 1987).

Coccolith assemblages were investigated at low resolution in order to validate the AMS ^{14}C and δ^{18}O-based stratigraphical framework of the four studied cores. Smear slides were prepared from the fraction <63 μm and examined by means of standard light microscope techniques under crossed nicols and polarized light at 1000× magnification. In order to improve the stratigraphic resolution of the Pleistocene interval, the biohorizons described for ODP leg 175 (Wefer et al., 1998) were utilized. This was in addition to the classic first/last occurrences (FO/LO) of index species, which include dominance intervals of single-species/taxonomical categories.

4. Results

4.1. LBB northern slope morphology and periplatform drift geometry

The LBB northwestern slope becomes a plateau-like structure over 4 km at ~40 m water depth (Fig. 4). The flat plateau-like structure is oriented parallel to the edge of the LBB and is considered as its margin. Slope angles divide the slope into different sections: the uppermost slope, the upper slope, the middle slope, and the lower slope. The uppermost slope (Rankey and Doolittle, 2012) extends between 40 and 300 m water depth with a mean slope angle of 1.15°, ~3.8° from 40 to 180 m and 0.6° from 180 to 300 m water depth. The upper slope extends from 300 to 650 m water depth with a mean slope angle of ~0.7. The middle slope extends from 650 to 800 m water depth with a mean slope angle of ~1.2. Finally, the lower slope extends from 800 to 900 m water depth with a mean slope angle <~0.5 (Fig. 4).

The VHR seismic data (lines 110 and 001) of cruise CARAMBAR 1.5 showed a very high amplitude signal corresponding to the sea floor and continuous layered sub-bottom reflectors below (Fig. 4). At the base of the uppermost slope, a surficial acoustically-transparent echofacies related to a low signal penetration was observed down to ~400–500 m water depth. This shallow transparent echofacies (in red in Fig. 4) thins basin-ward with a maximum thickness of 9 m at approximately 180 m water depth. Below this transparent echofacies, distinct continuous and subparallel internal reflectors were observed to 800 m water depth (in blue in Fig. 4). This unit has been previously described by Tournadour et al. (2015) as Unit G, which was not part of the LBB Drift according to seismic data (Fig. 3). These authors defined the LBB Drift as restricted to seismic Unit F (Fig. 3). The base of Unit G is defined by a continuous erosional surface associated with punctual mounded topographies and characterized by hyperbolic echofacies (Fig. 3). The frontal and lateral terminations of the LBB Drift (at ~800 m water depth) were affected by several submarine slides. The frontal part of the periplatform wedge forming the Unit G presents a thickening which suggested the influence of along-slope processes (Fig. 3). Unit G fills the topographic depressions induced by mass transport complexes and frontal submarine slides and it thins basinwards. Linear incisions visible on the sea floor evidence ancient frontal slides in present-day bathymetry that are not completely filled by the sediment of Unit G (Fig. 3).

4.2. Other morphological surface features related to the Antilles Current in the northern LBB slope

Specific mound-like features also occur on the sea floor of the LBB slope. They are interpreted as coral mounds (overlapping hyperboles in VHR seismic). Sedimentation surrounding the deep coral mounds was not symmetric along the strike profile and, showed a preferential accumulation on the eastern side of the coral mounds (Fig. 4). The presence of coral mounds between 600 and 800 m water depth insisted on the presence of bottom currents as deep-coral growth requires a regular supply of nutrients usually brought by these currents (Correa et al., 2012). Moreover, the coral's present spatial distribution is associated

with the topography. This is because coral mounds are typically located on indurated topographic highs (blocks or ridges) that serve as substrate for coral larvae settlement (Correa et al., 2012). Distribution of coral mounds during the Cenozoic seems related to major erosional surfaces described in Tournadour et al. (2015; Fig. 3). Escarpments related to these surfaces would have formed topographic highs that could be preferentially used as substrate for coral mounds.

The asymmetric sediment accumulation around the coral mounds, namely, non-deposition on the western side of the cold water mound and preferential deposition on the eastern side (Fig. 3), suggested that settling of fine-grained particles was driven by bottom currents locally trapped against escarpments. This induced non-deposition areas behind the coral mounds. These asymmetrical depositional structures are interpreted as "comet-like structures" that resulted from westward-orientated bottom currents such as the Antilles Current. Therefore, this provided evidence that the Antilles Current is present along the seafloor up to 800 m water depth in the northern LBB slope.

The presence of the Antilles Current in the study area was also evidenced by 1 to 2 m-long erosional structures on the sea floor oriented in a northwestern direction in the northern lower slope of LBB (Tournadour, 2015). In particular, the presence of sediment starved ripples in these intermounded areas east of the study site implied the presence of a strong current (Mullins et al., 1981). During the CARAMBAR 1.5 cruise, six sound velocities profiles were collected (only 4 are shown) that suggest the presence of two different water masses: one from 0 to 150 m and one from 150 to at least 1000 m water depth, which may be related to the Antilles Current (Fig. 2). This suggested that the Antilles Current remobilized the sediment in the eastern part of the north LBB slope, and promoted deposition in the western part of the slope of the LBB Drift.

4.3. Sediment features in the northern LBB slope

The CARG-27 sample was collected on a plateau-like structure, located on the margin of LBB. It is an indurated calcareous block (16 × 11 × 7 cm) with living algae, tubes of serpulidae, crustose red algae and moldic pores on its surface (Fig. 5A). The block contains benthic foraminifera such as *Amphistegina* and miliolids, some bivalves, *Halimeda* plates, gastropods, and otoliths. All the components were cemented and voids due to moldic dissolution were rounded with 1 cm diameters.

Core CARGC-28 was collected in the thickest part of shallow transparent facies, on the uppermost slope. Sediment was not fully recovered, probably due to technical problems during coring operations. This core contained two types of sediments. First, the basal layer (1 cm-thick) consisted of broken *Halimeda* plates (~35%) and benthic foraminifera (~35%) associated with a few (~10% each) planktonic foraminifera, bryozoan clasts and undetermined bioclasts. Second, the top layer (1 cm-thick) was made of pellets (~50%) with benthic foraminifera (~35%) associated with rare specimens of planktonic foraminifera, broken *Halimeda* plates (~1–2 mm), bivalves and bryozoan clasts. In both units, the benthic foraminifera were a mixture of deep and shallow bank-derived specimens such as *Amphistegina* sp., *Peneroplis* sp. and *Homotrema rubrum*. The matrix (<20 μm) was dominated by aragonite needles associated with rare (~2–3%) coccoliths.

Core CARKS-18 was also collected in the shallow transparent facies and showed three sedimentary layers (Fig. 6). Layer 1 extended from the base of the core to 85 cm, and showed a light gray grainstone with cm-scale indurated nodules mixed with mainly planktonic foraminifera and pteropods. Grain-size measurements showed that the coarsest sediment had a D50 up to 475 μm (Fig. 6). Thin sections indicated the presence of several indurated nodules with different sizes (Fig. 6B). Some of them contained planktonic fauna such as foraminifera or pteropods (Fig. 6C). SEM images of the surfaces of some indurated nodules showed euhedral crystals of calcite ranging from 2 to 5 μm (Fig. 5B). At first glance, the size of the indurated nodules decreased toward the top of the layer. Tests of the planktonic organisms appeared mostly yellow (a small number remained white), and not broken. This layer was interpreted as a diagenetic sequence. Layer 2 extended from 85 cm to 34 cm. It was a light gray bioturbated wackestone corresponding to a typical periplatform ooze. Abundance of aragonite needles was observed in SEM images (Fig. 5C). Layer 3 extended from 34 cm to the top of the core. It was a light gray packstone with an erosive base showing a coarse grain-size between 34 cm and 30 cm, and a finer grain-size from 30 cm to the top of the core. This poorly sorted fining-up sequence was interpreted as a turbidite.

Cores CARKS-20 and CARKS-21 were localized in the distal part of Unit G in the middle slope. They both showed 1 to 3 m-thick beds of white to light gray fine wackestone (D50 between 15 and 20 μm) interbedded with medium/coarse wackestone to packstone beds (D50 between 30 and 160 μm) of 10 to 120 cm in thickness (Figs. 7, 8). Sediments in cores CARKS-20 and CARKS-21 showed bioturbated typical

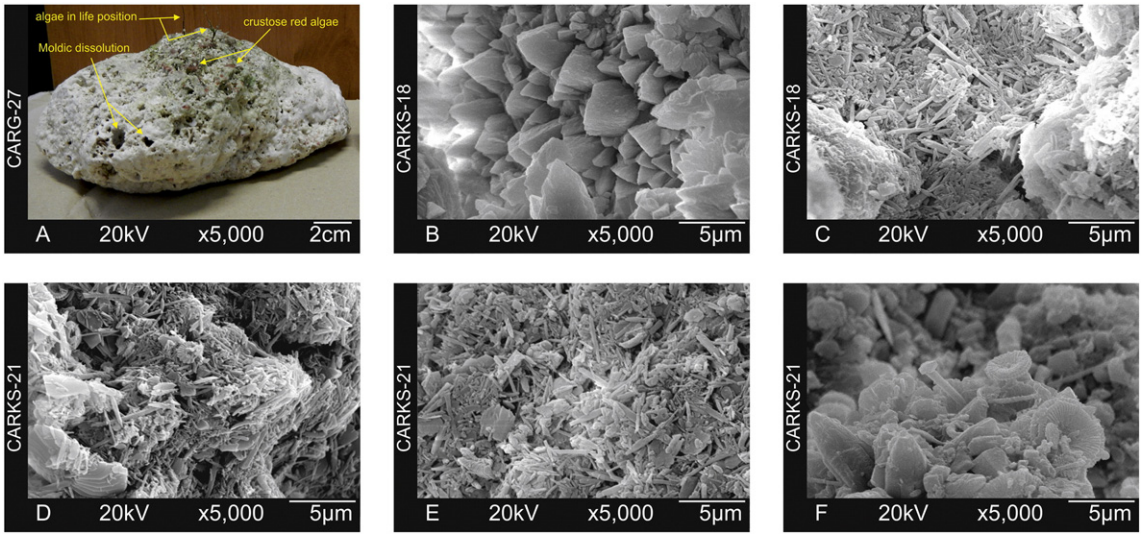

Fig. 5. A) Photo of the indurated calcareous block of CARG-27; B–F: SEM images. B) Lithified nodule (100 cm in CARKS-18); C) fine-grained sediment (46 cm in CARKS-18); D) fine-grained sediment (301 cm in CARKS-21); E) coarse-grained sediment (375 cm in CARKS-21); F) slightly-indurated sediment (1193 cm in CARKS-21). Note the presence of distinct aragonite needles and coccoliths.

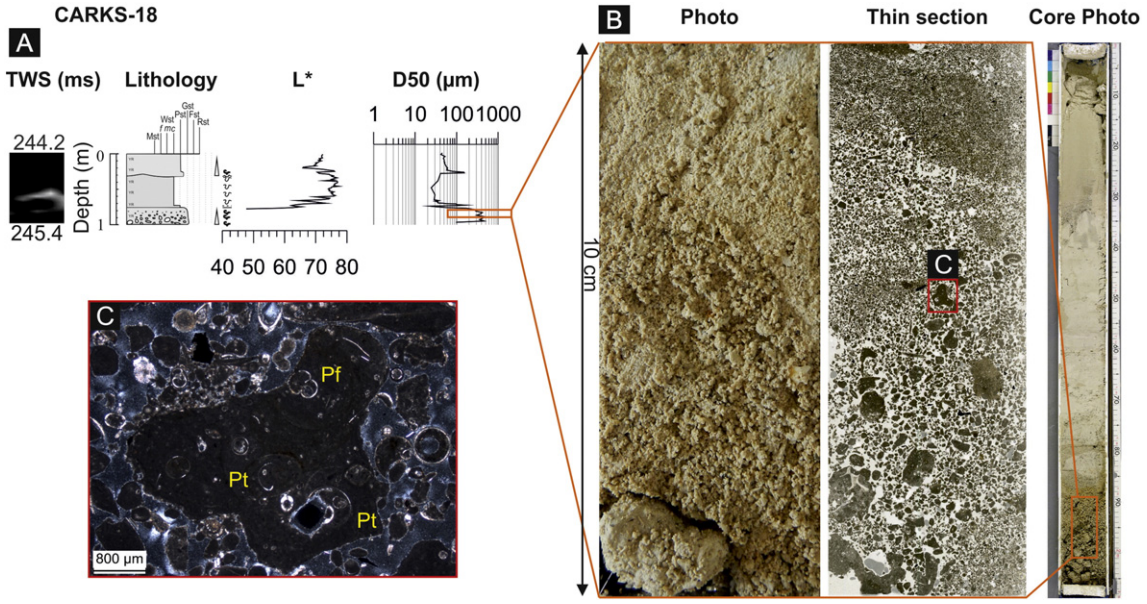

Fig. 6. A) CARKS-18 correlations between CHIRP data in TWS (ms) and lithology, parameter L* and grain-size measurements; B) photo and thin section of the 10-cm grainstone interval and photo of core CARKS-18; C) enlarged microphoto of one indurated nodule from the thin section taken with a ×25 magnification. Pt: Pteropods, Pf: Planktonic foraminifera.

periplatform ooze sediment with a majority of planktonic foraminifera, pteropods, and a few benthic foraminifera mixed in a carbonate matrix made of aragonite needles and coccoliths (Figs. 7, 8, 5D, E). Carbonate content comprises approximately 90% of the sediment particles except in the clay-rich intervals where it reaches 60%. SEM images showed a high abundance of aragonite needles (2–3 μm long; 0.25 μm width) in fine-grained sediment, but a lesser abundance in coarse-grained sediment that showed a higher content of aragonite blades (4–5 μm long; 0.45 μm width). These aragonite blades were twice as wide as aragonite needles (Fig. 5D, E). In both cores CARKS-20 and CARKS-21, the

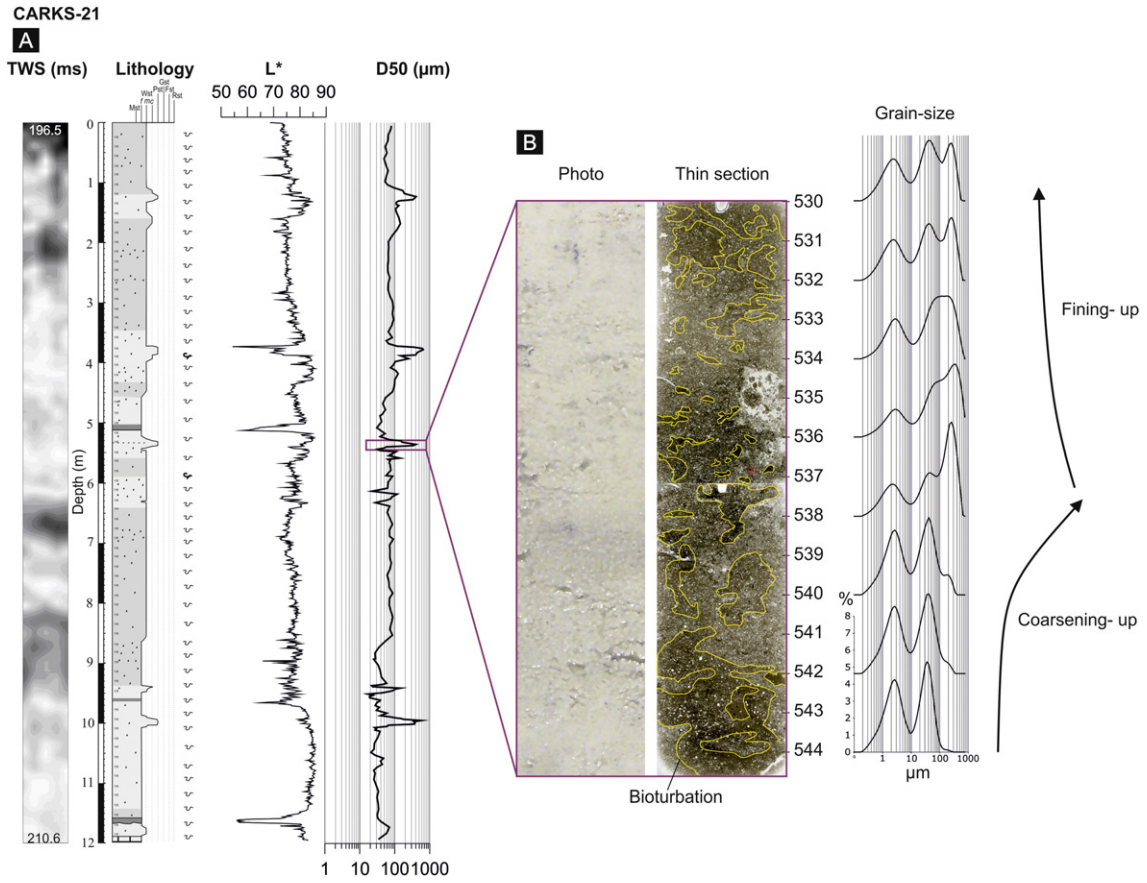

Fig. 7. A) Core CARKS-21 correlation between CHIRP data in TWS (ms), lithology, parameter of sediment brightness L* and grain-size median; B) photo, thin section and grain-size modes of the 15 cm-long interval with wackestone to fine packstone showing a coarsening-up unit followed by a fining-up unit. Bioturbations are highlighted by yellow lines on the thin section.

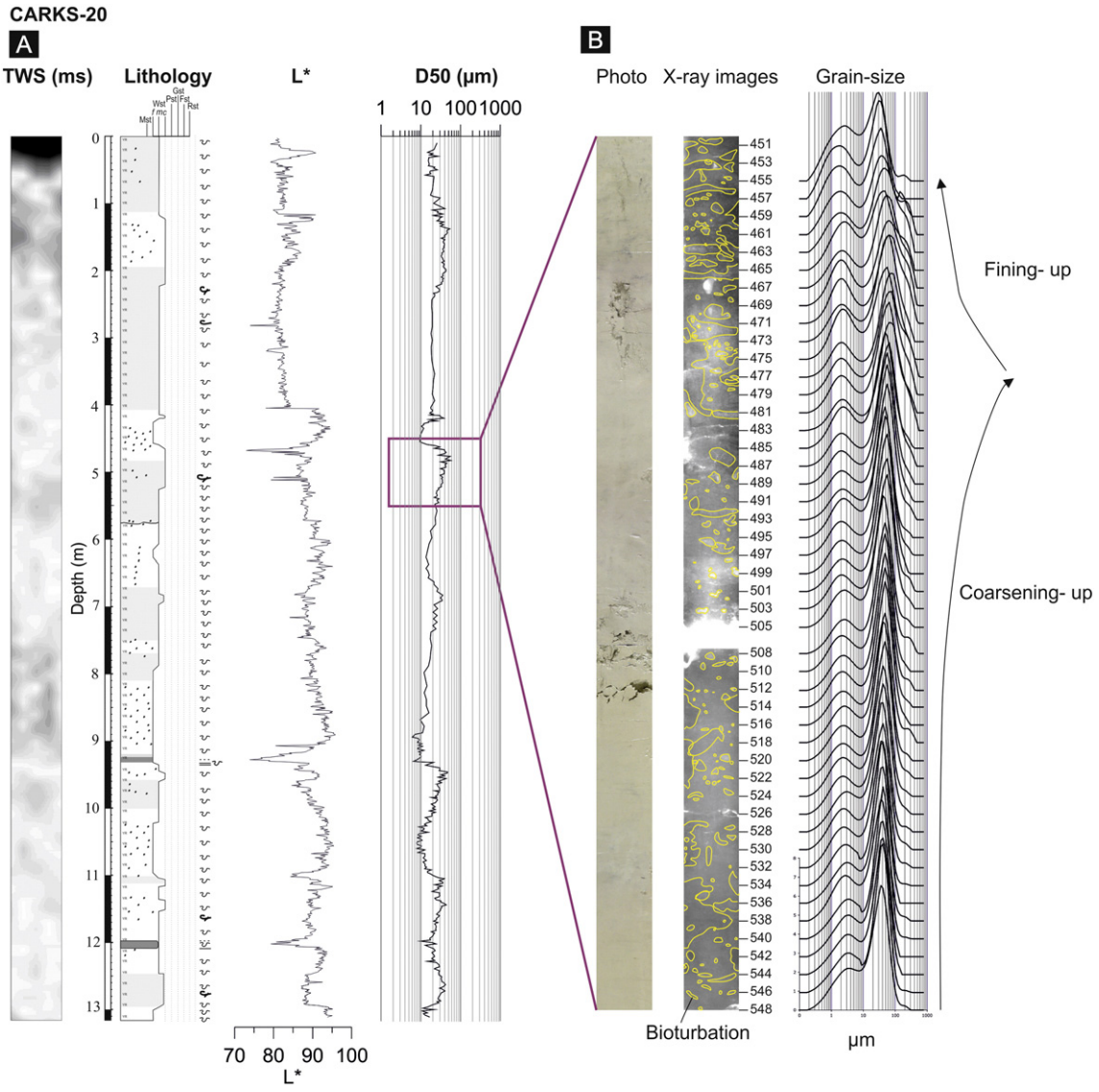

Fig. 8. A) Core CARKS-20 correlation between CHIRP data in TWS (ms), lithology, parameter of sediment brightness L* and grain-size median; B) photo, X-ray images and grain-size modes of the 98 cm-long interval of wackestone showing a coarsening-up unit followed by a fining-up unit. Bioturbations are highlighted by yellow lines on X-ray images.

coarsest-grained beds showed a coarsening-up unit followed by a fining-up unit forming a distinct bigradational sequence. In core CARKS-21, the D50 curve showed coarser sediments over a shorter sequence than in core CARKS-20, suggesting condensed deposits in CARKS-21. The base of CARKS-21 (~30 cm) was slightly lithified and showed 2 to 6 μm-long euhedral calcite crystals (Fig. 5F).

4.4. Stratigraphy of the cores

4.4.1. Stratigraphy of the reference core: CARKS-21

CARKS-21 was chosen as the reference core because it is the only core which penetrates through the entire layered drift deposits at its distal fringe (Figs. 3, 4). Calcareous nannofossil biostratigraphy highlighted the presence of five acme zones: the acme of *Emiliania huxleyi* from MIS 1 to MIS 4/5b; the transitional acme of *E. huxleyi* and *Gephyrocapsa aperta* from MIS 4/5b to the top of MIS 6, the acme of *G. aperta* from the top of MIS 6 to the base of MIS 8, the acme of *Gephyrocapsa caribbeanica* between the bases of MIS 8 and MIS 15, and the acme of small *Gephyrocapsa* between the bases of MIS 15 and MIS 25. The last occurrences (L.O.) of *Pseudoemiliania lacunosa* and *Reticulofenestra asanoi*, indicate an age of 458 kyrs BP (Thierstein et al., 1977) and 830 kyrs BP (Sato et al., 1991), respectively. From 9.3 m to the base of the core, the sediments represented ca 500 ka of sedimentation over 2.65 m, so calcareous nannofossil biostratigraphy suggested low sedimentation rates (0.5 cm/ka) and/or perturbation.

$\delta^{18}O$ values based on *G. ruber* var. *alba* tests ranged from −1.86 to 0.69‰ (Δ2.55). These values agree with previous results published for the Bahamas (Droxler et al., 1983; Boardman et al., 1986; Lantzsch et al., 2007). The $\delta^{18}O$ curve was correlated from the top of the core to 9.3 m with the $\delta^{18}O$ benthic stack of Lisiecki and Raymo (2005). However, no correlation was possible with the $\delta^{18}O$ benthic stack because the base of the core to 9.3 m showed perturbation and/or low sedimentation rates.

The $\delta^{18}O$ curve of CARKS-21 presented a slightly different shape than the $\delta^{18}O$ benthic stack of Lisiecki and Raymo (2005) during MIS 5 and MIS 7. This can be explained by the high variability in sedimentation rates between glacial and interglacial periods. Indeed, the short sea-level lowstand during MIS 7 was likely associated with bioturbated and condensed deposits making the detection of the $\delta^{18}O$ changes difficult with the chosen sampling resolution step (10 cm intervals between each samples).

The strontium curve values ranged from 33,209 ppm to 224,189 ppm and calcium element content was always >90% except in the clay-rich intervals (not shown). The Sr/Ca ratio showed a clear positive correlation with the $\delta^{18}O$ signal along the first 9.3 m (Fig. 9). Infrequent anomalies in the correlation were located in the clay-rich intervals corresponding to a change in sediment nature. Strontium was incorporated as a minor component (2000–10,000 ppm) during the formation of biogenic carbonates, representing 1% in aragonite materials and 0.1 to 0.2% in calcite materials (Morse and MacKenzie, 1990). Most of the bank-derived materials, such as calcareous algae, corals, and ooids, and 80% of the aragonite needles had a high content of Sr–aragonite. However, pelagic organisms derived from the water column had a high content of low-Mg calcite (planktonic foraminifera, coccoliths) and a few low-Sr aragonite (pteropods and benthic molluscs) (e.g. Veizer, 1983; Boardman and Neumann, 1984; Shinn et al., 1989; Morse and MacKenzie, 1990). In the processed cores, the strontium signal mostly represented the quantity of strontium in aragonite and allowed for distinguishing between aragonite exported from the bank-top and aragonite formed in the pelagic water column (Boardman and Neumann, 1984). The strontium signal was an indicator of relative sea-level in this almost pure carbonate environment (Boardman et al., 1986).

The two radiocarbon ages of 10,553 cal yrs BP at 98 cm and 35,796 cal yrs BP at 138 cm constrain the Holocene and MIS 3. However, a third date on a sample collected at 20 cm was rejected while its age assignment was considered as too old compared to other stratigraphic results (Fig. 9).

4.4.2. Stratigraphy of the others cores: CARG-28, CARKS-18 and CARKS-20

In core CARKS-20, no specimen of *P. lacunosa* was found, indicating that the core does not reach MIS 12. The three radiocarbon ages of 3279 cal yrs BP at 20 cm, 4427 cal yrs BP at 60 cm and 18,042 cal yrs BP at 94 cm were consistent with the presence of MIS 1 and 2 at the top of the core (Fig. 10). The strontium curve ranged from 65,729 ppm to 244,328 ppm (not shown) and the ratio Sr/Ca displayed the same trends as for CARKS-21. Variations in the strontium content were in agreement with the calcareous nannofossil biostratigraphy and allowed defining MIS 1 to 11 (424 ka; Lisiecki and Raymo, 2005, Fig. 10).

In core CARKS-18, only the acme of *E. huxleyi* from MIS 1 to MIS 4/5b was detected in the non-perturbed intervals located between 40 cm and 70 cm but no reliable data was obtained in the basal and top layers. In the basal layer, a glacial faunal assemblage was observed based on the increase of *Globorotalia inflata* and *Globigerina falconensis* and the absence of *Globorotalia menardii menardii* (Kennett and Huddleston, 1972; Ericson et al., 1964; Beard, 1969, 1973; Ruddiman, 1971; Poag and Valentine, 1976; Martin et al., 1990). The strontium values range between 45,052 and 202,938 ppm and the ratio Sr/Ca showed a complex pattern in the top layer because of the presence of a turbidite. The stratigraphical analyses suggested glacial sediments from the base to 72 cm, most likely MIS 2, and Holocene sediments from 72 cm to the top (Fig. 11).

In core CARGC-28, a Holocene faunal assemblage was observed based on the presence of interglacial planktonic foraminifera and the absence of *Globorotalia menardii flexuosa*. The last occurrence of the latter appeared approximately 80 to 90 kyrs cal BP (Bolli and Saunders, 1985).

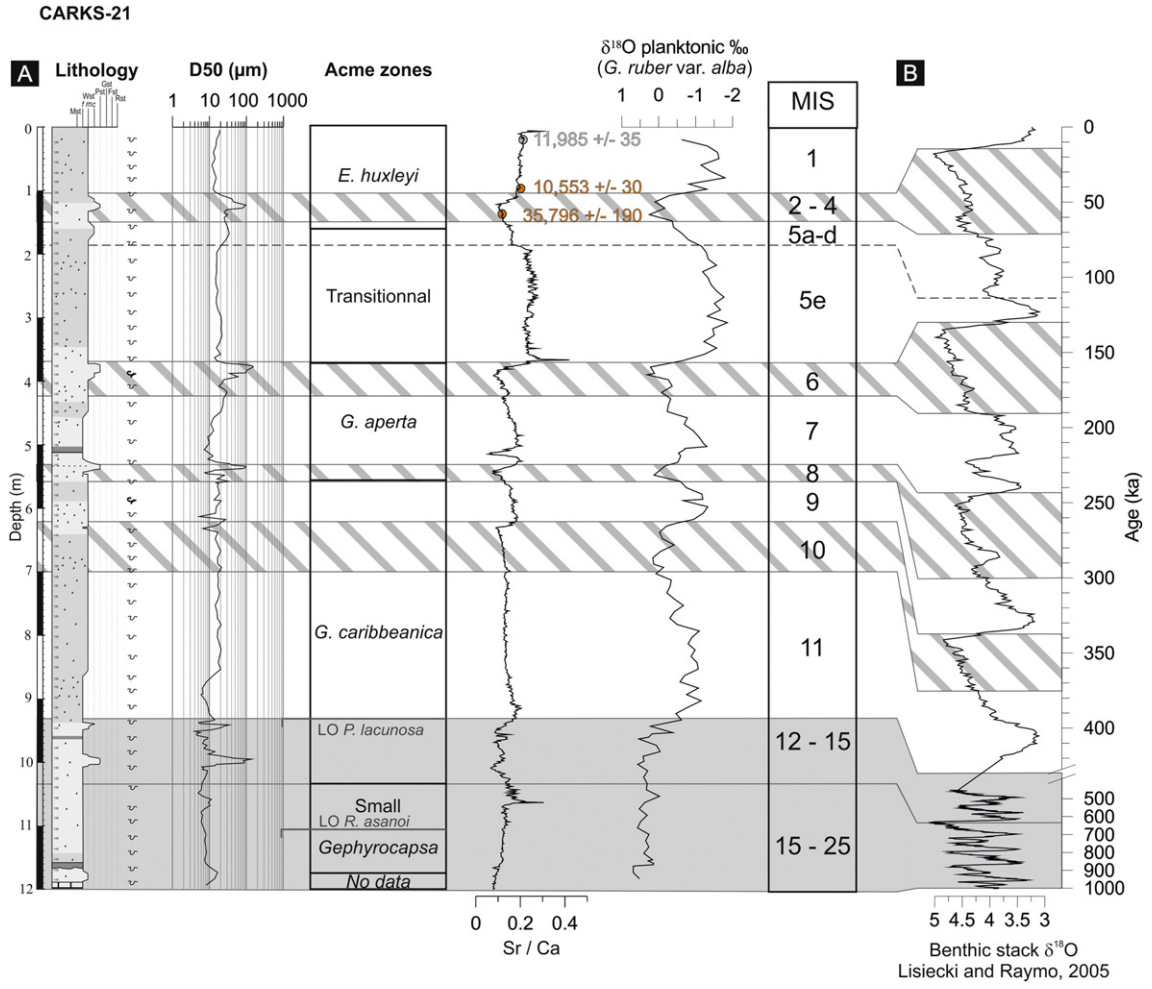

Fig. 9. Stratigraphy of core CARKS-21 with A) lithology, grain-size median, coccolith acme zones, Sr/Ca ratio from XRF core scanner, $\delta^{18}O$ planktonic and interpretation of the MIS boundaries; B) Benthic stack LR04 of Lisiecki and Raymo (2005). The three AMS radiocarbon dates with their error are indicated in yrs cal BP along the Sr/Ca curve. Distinct variations in sediment input can be observed for glacial periods (cross-hatched intervals) and interglacial intervals with higher accumulation rates and lighter stable isotope values during interglacial time periods.

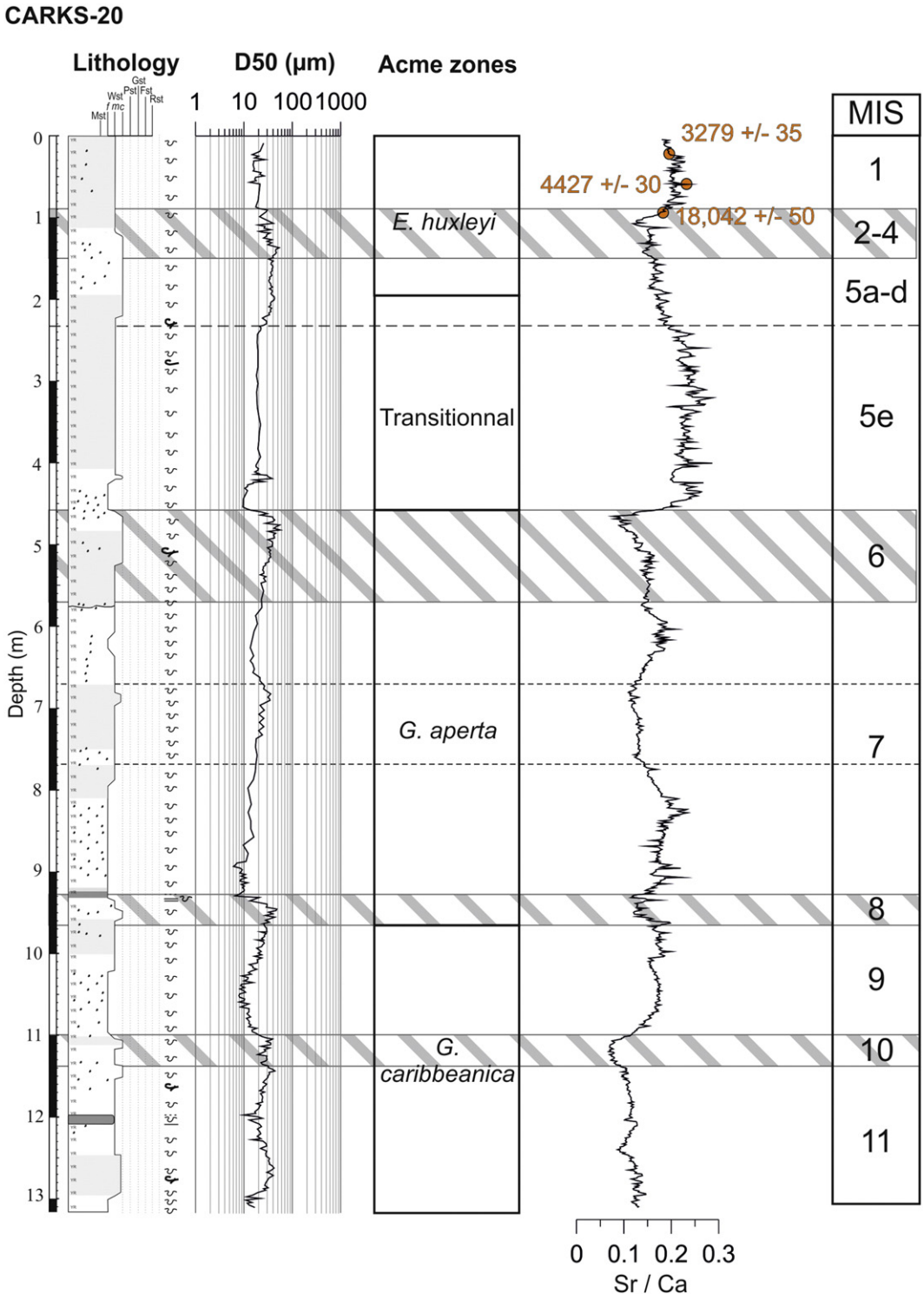

Fig. 10. Stratigraphy of core CARKS-20 with A) lithology, grain-size median, coccolith acme zones, Sr/Ca ratio from XRF core scanner and interpretations of MIS boundaries. The three AMS radiocarbon dates with their error are indicated in yrs cal BP along the Sr/Ca curve. Distinct variations in sediment input can be observed for glacial periods (cross-hatched intervals) and interglacial intervals with higher accumulation rates and lighter stable isotope values during interglacial time periods.

5. Discussion

5.1. Flooding periods with RSL > −6 m

The LBB lagoon is very shallow (water depth between 1 and 5 m), except in the far northwestern part where the platform top deepens to 6–12 m. The average water depth of the lagoon is less than 6 m (Williams, 1985). The −6 m bathymetric curve was used in order to define the flooding periods based on RSL curves of Miller et al. (2011) and Siddall et al. (2003; Fig. 12). The last flooding period was the most constrained. For example, the limit of 6 m below modern sea level corresponded to ~5 cal kyrs BP and 90% of the LBB was flooded around

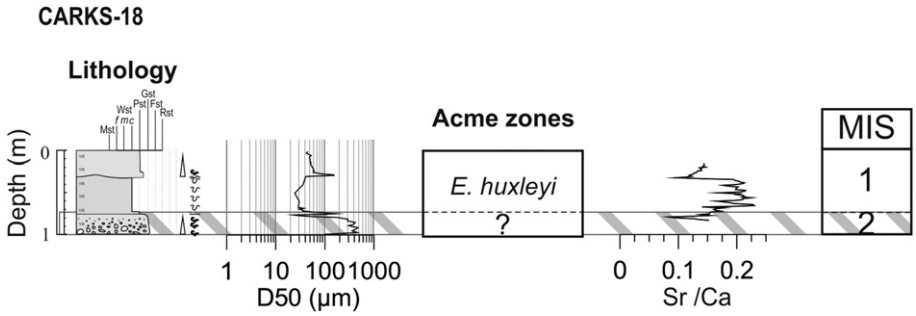

Fig. 11. Stratigraphy of core CARKS-18 with A) lithology, grain-size median, coccolith acme zone, Sr/Ca ratio from XRF core scanner and interpretations of MIS boundaries. Grainstone interval developed from the base to 72 cm likely during MIS 2 and wackestone to packstone intervals developed from 72 cm to the top the Holocene. The ratio Sr/Ca shows a complex pattern on the top unit which is related to the turbidite and not to a stratigraphical signal.

4 cal kyrs BP (Droxler et al., 1983). In this study, the basal limit for the last flooding period given by the ^{14}C age on core CARKS-20 at 60 cm at 4.427 ± 30 cal kyrs BP was used.

Throughout the last 424 ka, three major flooding periods exceeding 6 m water depth were defined based on the aforementioned RSL curves. These periods coincided with specific time intervals during MIS 1, MIS 5 and MIS 11 (orange areas in Fig. 12). These major flooding periods matched those detected in cores GB1 and GB2 on Gran Bahama Island (McNeill et al., 1998) and outcrops on New Providence Island (Aurell et al., 1995). On the margin, an indurated block (CARG-27) was found on the surface that was not covered by unlithified sediment and was associated with high amplitude surface reflectors in the seismic profiles (Fig. 4). This suggested that at present limited shallow carbonate sediments had accumulated on this part of the margin and that sediment can be easily diagenetized. As only one sample was taken, it was difficult to generalize this observation. Further, this block could be related to block failures from the shallower escarpment.

During the three major flooding periods, aragonite needles were the main constituent of the sediments along the entirety of the slope with only a few planktonic organisms present. These included foraminifera, a few pteropods and rare coccoliths. Aragonite needles were likely derived from the platform where abundant strontium-rich aragonite needles have been observed (Neumann and Land, 1975). The flooding periods showed sedimentation rates averaging ~17 cm/ka (Table 2) with higher values found in core CARKS-20 (up to ~32 cm/ka during MIS 5e). These high sedimentation rates observed along the core profile were related to high carbonate production on the platform (Figs. 13A, 14A). Off-bank transport allowed a five to nine times higher accumulation (Table 2) of fine-grained carbonate sediment (aragonite needles) over the middle slope (CARKS-20/21) during periods when the bank-top was flooded (12 to 23 cm/ka). This was substantially increase compared to when the shallow top is exposed (1 to 4 cm/ka). In addition, aragonite needles were transported off-bank and spread over the entire slope (Fig. 13A). Over the last 424 ka, the three major flooding periods represented a cumulated duration less than 25 ka (4.4 ka, 7 ka and 12 ka for MIS 1, MIS 5 and MIS 11, resp.). This indicated that maximum production periods of shallow carbonate on the platform corresponded to ca 6% of the time over the last 424 ka.

Off-bank transport processes are often used to explain the sedimentation patterns along carbonate slope environments (e.g. Heath and Mullins, 1984; Rendle et al., 2000; Rendle-Bühring and Reijmer, 2005; Roth and Reijmer, 2005). On the LBB, present-day off-bank transport of fine sediment occurs preferentially along leeward margins, i.e. on the west and south sides of LBB (Hine and Neumann, 1977; Hine et al., 1981a, 1981b). Results of this study showed that this off-bank transport was also significant along the windward margin of LBB. Off-bank transport thus corresponded to the sink of sediment-laden mesopycnal and hyperpycnal platform-initiated water flows. These water flows reach their density equilibrium depth (i.e. compensation depth), around a maximum of 400–800 m water depth in the Bahamas (Wilson and Roberts, 1992, 1995). A phenomenon called density cascading, which includes an increase in shallow-water bank density (Wilson and Roberts, 1992, 1995) can be triggered in both winter and summer months. In winter, density cascading is driven by cold fronts (Fernandez-Partegas and Mooers, 1975; Bosart and Schwartz, 1979; Roberts et al., 1982) and in summer by intense heating and evaporation associated with storms (Dill and Steinen, 1988; Shinn et al., 1993). Monitoring of sediment traps shows that these dense platform flows can spread easily over 20 km (Hickey et al., 2000), and potentially over 50 km (Pilskaln et al., 1989), covering the entire slope of the LBB Drift (Fig. 13A). Fine-grained sediment settles rapidly to the adjacent slopes (Boardman and Neumann, 1984; Pilskaln et al., 1989; Wilson and Roberts, 1992), suggesting acceleration of sediment settling by aggregation with zooplankton fecal pellets (Boardman and Neumann, 1984) or macro-aggregate formations with aragonite needles (Pilskaln et al., 1989). Bottom currents influence the eastern side of the LBB Drift, allowing the survival of coral mounds, but their influence is limited during interglacial periods, preventing winnowing of fine-grained sediment and their dispersion by current over great distances. The high accumulation of periplatform oozes during these maxima of platform flooding prevents circulation of interstitial waters through the sediment that is essential for early stages of marine diagenesis commence (Bathurst, 1975).

5.2. Interglacial periods with RSL between −6 m and ca −90 m

During most of the interglacial periods, RSL was not high enough to flood the shallow-platform. However, when RSL was only 40 m lower than the present-day sea level, shallow carbonate sediment production was restricted to the margin rims of the present LBB (Fig. 13B, 14B). The northwestern margin of LBB is a plateau-like structure located at about −40 m (Fig. 4). This was previously observed in other seismic profiles collected on the western side of the LBB Drift over a width of approximately 4 km (Hine and Neumann, 1977). The presence of *Halimeda* plates and shallow-water benthic foraminifera in the indurated CARG-27 block suggested shallow-water carbonate production on the margin when the platform was exposed. Observations of such indurated blocks with similar components (*Halimeda* sp.) were observed on the cemented slope of Tongue of the Ocean (TOTO, Grammer and Ginsburg, 1992; Grammer et al., 1993). The components and the syndepositional cements were dated between 14,000 to 10,500 years ago by radiocarbon measurements (Grammer and Ginsburg, 1992), corresponding to the last interglacial periods before the onset of the major flooding of MIS 1. Despite the deeper depth of the cemented slope of TOTO (from ~120/130 at the base of the platform edge wall to 365 m water depth), this results is consistent with the hypothesis that production and cementation occur on the LBB margin (at 20 to 40 m water depth) when the shallow-water platform was not flooded.

During these interglacial periods corresponding to an exposed platform, sediments observed along the northwestern LBB slope contained

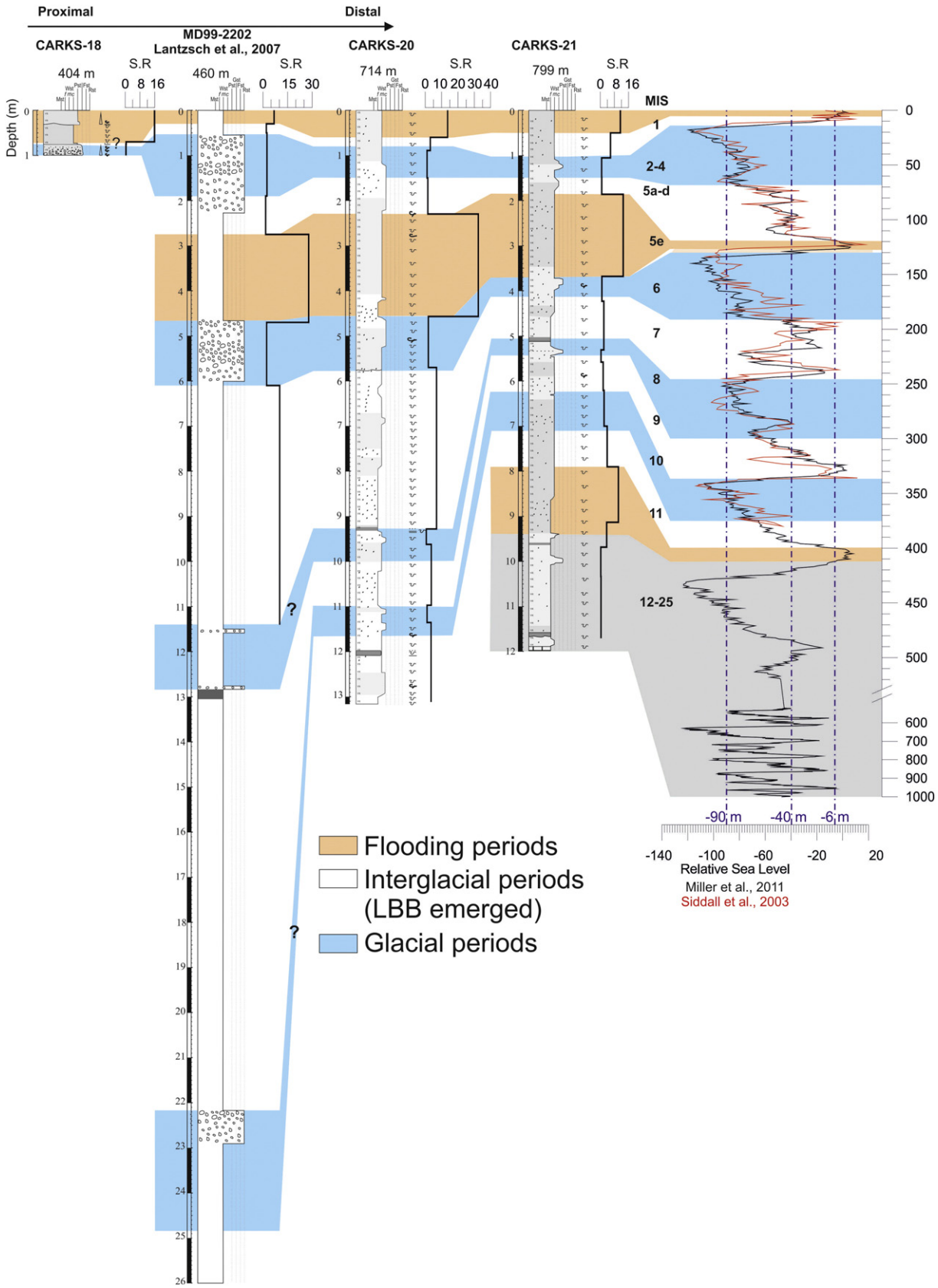

Fig. 12. Log correlation between cores CARKS-18, MD99-2202, CARKS-20, CARKS-21 and relative sea-level curves from Miller et al. (2011; black curve) and Siddall et al. (2003; red curve). Sedimentation rates (S.R.) are added on the right side of the log for each core. Orange areas indicate flooding periods of LBB; white areas correspond to interglacial periods when LBB was emerged, and the blue areas are related to the glacial periods. Gray area indicates periods with low sedimentation rates observed in CARKS-21 without major flooding periods. In the case of MD99-2202, stratigraphy of MD99-2202 may be biased before MIS 7 due to an erosional surface highlighted in Tournadour et al. (2015) so stratigraphic correlations before MIS 7 were highlighted by the symbol "?".

Table 2
Average sedimentation rates (cm/ka) for the different cores through time. It should be noted that sedimentation rates during the flooding periods of MIS 1 may be slightly biased because it is still flooded, and sedimentation in core CARKS-18 has been perturbed by turbidity currents (Fig. 3). As MIS 7 and MIS 9 are not flooded during a period enough long and RSL was not enough high, limit between flooding and exposed interglacial periods could not be separated.

Average sedimentation rates (cm/ka)	CARKS-18	MD99-2202	CARKS-20	CARKS-21
Flooding interglacial periods				
(RSL > 6 m)	16	18	23	12
MIS 1	≥16	≥7	≥14	≥11
MIS 5e	–	28	32	13
MIS 11	–	–	–	10
>Exposed interglacial periods				
(90 < RSL < 6 m)	0.5	10	4	3
MIS 1	0.5	2	3	6
MIS 5a–d	–	1	2	0.8
MIS 7	–	10	7	2
MIS 9	–	–	4	2
MIS 11	–	–	–	4
Exposed glacial periods				
(RSL < 90 m)	0.4	4	1	1
MIS 2–4	≥0.4	3	1	0.7
MIS 6	–	2	2	0.9
MIS 8	–	2	0.6	0.5
MIS 10	–	–	1	2

*Indicates values to take with caution. In the case of CARKS-18, because the unit corresponding to the MIS 2–4 sediment is not complete, so the sedimentation rate given for the MIS 2–4 is a minimum. In the case of MD99-2202, stratigraphy of MD99-2202 may be biased before MIS 7 due to an erosional surface highlighted in Tournadour et al. (2015) so sedimentation values from MIS 8 to MIS 10 are not indicated.

a larger number of planktonic foraminifera and pteropods that were mixed with aragonite needles and coccoliths. The sediment supply was reduced and sedimentation rates dropped to less than 4 cm/ka on average during these interglacial periods. Despite no major flooding during MIS 7, sedimentation rates for CARKS-20 were similar to those calculated for MIS 5 (Table 2). The latter is explained by differences in RSL fluctuations between MIS 5 and MIS 7. During MIS 5, RSL was characterized by one long period (~7 ka) with a very high sea level (more than −6 m) whereas during MIS 7 RSL was potentially characterized by 3 short periods (~1 ka each) with a high sea level (more than −6 m) according to the RSL curve of Siddall et al. (2003). The RSL curve of Miller et al. (2011) is different than that of Siddall et al. (2003), however it still suggested that during MIS 7 a relatively long period of time (~22 ka) RSL exceeded −40 m. It is likely that the 4 km wide plateau surrounding parts of LBB has provided a surface large enough to allow an active shallow carbonate sediment production that accumulated on the margin of the LBB during MIS 7. This shallow-water carbonate sediment production may be the source of the aragonite on the slope during periods of platform exposure (Boardman and Neumann, 1984), such as during MIS 5a–d. The same observation could be made for MIS 9 but only in core MD99-2202 which showed very high sedimentation rates (~25 cm/ka). It should be noted that stratigraphy of MD99-2202 may be biased before MIS 6 because of the presence of an erosion surface (Tournadour et al., 2015). RSL amplitudes during MIS 9 differ between the curve of Miller et al. (2011) and Siddall et al. (2003). Both studies agree that RSL must have been higher than −40 m for a relatively long period of time (~25 ka), which could allow shallow carbonate production on the margin of the LBB (Fig. 13B).

This restricted shallow carbonate sediment production most likely resulted in a reduced off-bank transport (Fig. 13B). Our study suggested that off-bank transport processes are the major sedimentary processes during these periods although the shallow carbonate production is limited to the plateau-like structure. Mixing between these bank-derived sediments and planktonic organisms, e.g. planktonic foraminifera, coccoliths and pteropods, explains the type of sedimentation observed (Figs. 13B, 14B). The velocity of the Antilles Current may not have varied drastically throughout the interglacial periods but its current cores (associated with highest velocities) likely deepened as the sea-level fell (Figs. 13B, 14B).

5.3. Glacial periods with RSL < ca −90 m and contourite sequences

Along the middle slope (~800 m water depth), sediments deposited during glacial periods corresponded to sediments (wackestone to packstone) coarser than those deposited during interglacial periods (Figs. 7, 8). These results ensured relationship between grain-size variations and glacial-interglacial cyclicity, which has been previously observed in cores located on the leeward and windward sides of GBB (Rendle et al., 2000; Rendle-Bühring and Reijmer, 2005). The coarser glacial sediments in both cores were characterized by thoroughly bioturbated sequences showing a coarsening-up unit followed by a fining-up unit (Figs. 7, 8). The increase of planktonic foraminifera and pteropods explained the coarsening-up trend of the unit. Fine-grained particles (<10 μm) represented less than 30% and sometimes less than 20%, and were mainly constituted by coccoliths mixed with aragonite needles and blades (Fig. 5E). Sedimentation rates dropped to less than 1 cm/ka in the studied cores, forming condensed intervals.

The observed depositional trends corresponded to the bigradational sequence of contourite defined by Gonthier et al. (1984). These coarse-grained contourites deposited during glacial periods developed as a result of increased winnowing of fine-grained particles by bottom currents (Fig. 13C). This observation suggested the influence of stronger bottom currents at 800 m water depth. This is thought to originate from the Antilles Current, which is a wind-driven current that may be strengthened during glacial periods, similar to what happened in the Straits of Florida (Brunner, 1975). In siliciclastic contourite depositional systems, where sedimentation rates during glacial periods were higher than during interglacial time periods, contourite sequences were described with millennial-scale variability related to the Dansgaard–Oeschger cyclicity (e.g. Llave et al., 2006; Voelker et al., 2006; Toucanne et al., 2012). The main difference between siliciclastic and carbonate contourite drifts was that this unique carbonate contourite sequence was very condensed (decimeter to meter scale) with very low sedimentation rates over the entire glacial period. However, typical diagnostic features of contourites such as grain-size distribution or bioturbation seem to be the same in both carbonate and siliciclastic deposits.

The contourite sequences were only observed along the middle slope suggesting maximum current velocities at approximately 600–800 m water depth during glacial periods, current velocities that were sufficiently high to sort sediments (Fig. 13C).

On the upper slope, glacial periods were characterized by grainstone deposition with foraminiferal sand and indurated nodules (i.e. cemented debris). The foraminiferal sand consisted of unbroken tests of planktonic foraminifera and some pteropods. The indurated nodules consisted of indurated micrite with hints of planktonic organisms. The nodules were interpreted as the result of increased carbonate cementation due to early stages of seafloor diagenesis. Similarly, on the western slope of GBB, well-lithified intervals (i.e. hardgrounds) were found almost exclusively within glacial intervals, when sedimentation rates were low, and interpreted to have formed on or close to the seafloor (at 308 and 437 m water depth; Malone et al., 2001). During glacial periods, the main sediment sources were low-Mg calcite-dominated sediment producers (e.g. coccoliths, planktonic foraminifera), which are less prone to early diagenetic processes while calcite is more stable than aragonite (Bathurst, 1975; Mullins et al., 1985). Hence, the diagenetic potential (Heath and Mullins, 1984) of the periplatform ooze was lower during glacial periods. Early marine cementation was likely related to two processes increasing the porosity of the sediment that acts simultaneously during glacial periods. First, it is thought that the decrease of sediment supply, especially fine-grained particles such as the aragonite needles, is the catalyst to initiate cementation. This

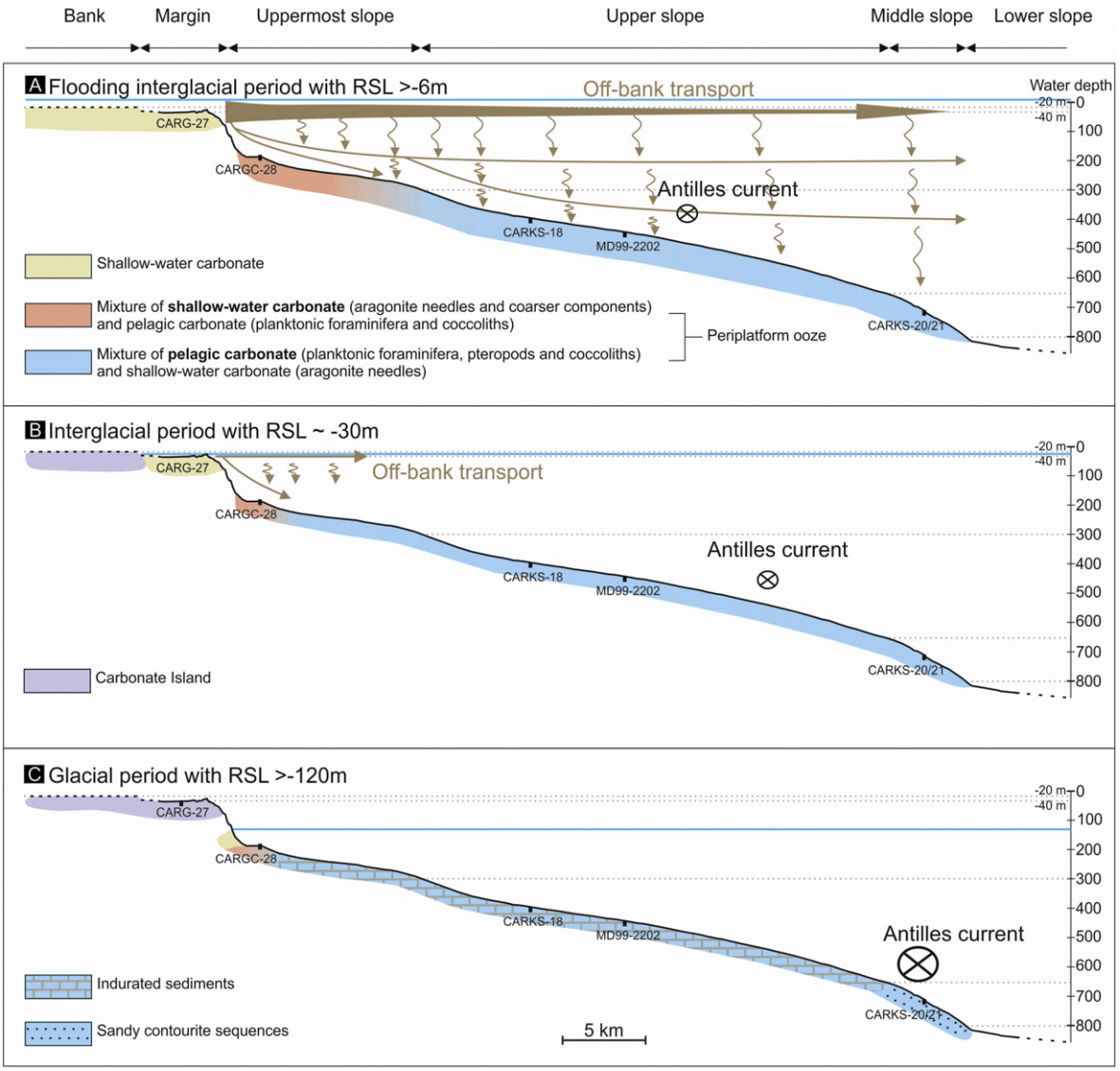

Fig. 13. Schematic diagrams illustrating the three different sedimentation patterns along the LBB periplatform drift over the last 450 ka: A) periods of major flooding of LBB with RSL around −6 m; shallow-water platform shows full sediment export; B) interglacial periods with partially emerged LBB and RSL around −30 m; shallow-water platform shows limited sediment export; and C) glacial periods with emerged LBB and RSL around −120 m; shallow-water platform is exposed and shows no sediment export. Deposit thickness is not to scale, but they indicate the general trend observed in the accumulation rates.

carbonate supply decrease is related to the sea-level fall and the reduction of the surface of shallow carbonate production to a narrow part of the photosynthetic zone on the uppermost slope. Second, the increase of the Antilles Current velocity related to the winnowing of the fine-grained sediments during glacial periods should not be downplayed. In both cases, higher porosity and lower sedimentation rates enhance circulation of interstitial waters through the sediment allowing more intense chemical, physical and biological reactions to take place that may stimulate cementation, and hence the formation of the indurated nodules (Bathurst, 1975).

The margin (<−40 m water depth) was completely exposed during glacial periods, as was the entire platform (Figs. 13C, 14C). The presence of moldic pores on the surface of the indurated block of CARG-27 (Fig. 5A) indicated a partial dissolution of it, a process that may occur at a time when the margin was exposed, so most likely during glacial periods. No data were collected from the uppermost slope covering the glacial interval due to bad penetration of CARG-28. However, it is suggested that on the upper slope, hard ground may be formed, similar to the eastern region of the study area (Mullins et al., 1984).

6. Conclusions

Results of this study showed that the sediment wedge of the northern LBB slope displayed the characteristics of a periplatform drift. The modern morphology of the LBB Drift corresponded to a zone affected by weak currents as described by the model of Betzler et al. (2014). This periplatform drifts was characterized by: 1) the vast input of carbonate sediment during highstands in sea-level, which export preferentially to the leeward side of the platform and, 2) the merging of the Antilles Current with the Florida Current, which shapes the northward-plastered contourite drift. However, the influence of these currents was probably limited to sediment redistribution processes during interglacial periods whereas it reworked the sediments from the entire slope during glacial periods. Further investigation is warranted to determine if the term “periplatform drift” may be used in past environment because it is difficult to morphologically highlight the influence of the current on the periplatform wedge with seismic tools.

Sedimentation variability along the slope, and through time during the last 424 ka showed three main periods: (i) the major flooding of

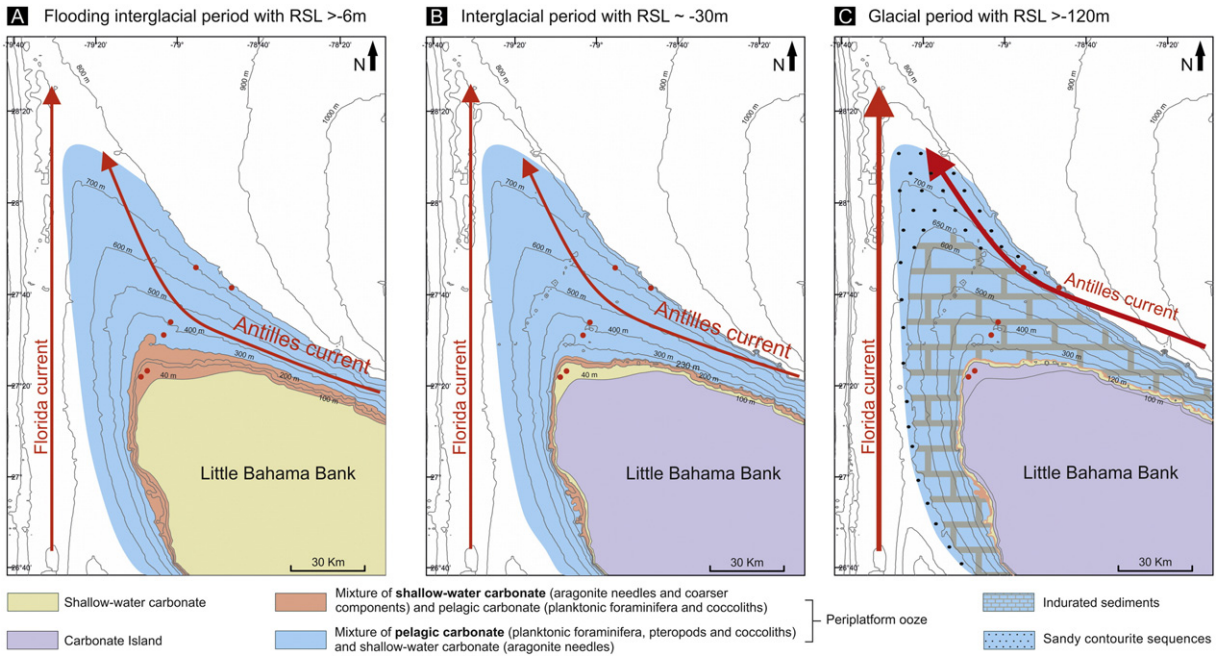

Fig. 14. Sketch with theoretical extension of shallow carbonate production and sediment deposition on LBB and its west northern slope for: A) flooding interglacial periods with RSL > −6 m; B) interglacial period with RSL around 30 m; and C) glacial periods with RSL > −120 m. Red dots correspond to marines cores used in this study. Isobaths are drawn after the General Bathymetric Chart of the Oceans (GEBCO, 2014) data set. As their resolution is 112 m, the −40 m isobaths delimit the platform for the margin and is drawn according to seismic profiles data (Hine and Neumann, 1977). Red arrows mark the direction of the main ocean currents.

LBB in interglacial periods, (ii) the interglacial periods with the partial emersion of the platform, and (iii) the glacial periods in which the sedimentation patterns differed in the uppermost (<300 m water depth), the upper (300–650 m water depth), and the middle slopes (650–800 m water depth). These differences in the sedimentation patterns were found to be the following:

1) Off-bank transport was the major sedimentary process during periods of major flooding of LBB. This allowed export of coarse bank-derived organisms and clasts (shallow benthic foraminifera, *Halimeda* plates, and likely pellets) toward the uppermost slope and of fine-grained particles (aragonite needles) over larger distances (up to 50 km). This leads to high accumulation rates along the entire drift (average ~17 cm/ka). Along the upper and middle slopes, the aragonite needles mixed with planktonic organisms (planktonic foraminifera, coccoliths, and pteropods) to form a typical, fine-grained periplatform ooze.
2) Low sea-level interglacial periods (onset of MIS 1, MIS 5a–d, MIS 7, MIS 9) in which the shallow-water portion of the platform was emerged, corresponded to limited shallow-water carbonate production and reduced sediment export toward the slope. When the relative sea level was above −40 m present bathymetry, shallow-water carbonate production was promoted over the 4-km large plateau-like structure and sediment was exported to the slope along preferential pathways.
3) Glacial periods and corresponding sea-level lowstands lead to exposure of the platform and drastic reduction of shallow-water carbonate production. Current-related deposits dominated during glacial periods along the northern Bahamas slopes over the last 424 ka. Along the upper slope, early marine cementation promoted the formation of nodules through mainly a decrease in sediment input and possibly the winnowing of fine-grained sediments by a stronger glacial Antilles Current. Along the middle slope, the Antilles Current transported sufficient nutrients to favor the development along the north-western part of LBB slope of cold-water coral mounds at water depths between 600 and 800 m. Between these coral mounds, the sediments consisted of coarser-grained periplatform ooze deposits that were characterized by thoroughly bioturbated bigradational sequences with a coarsening-up unit followed by a fining-up unit. This typical contourite sequence is known from siliciclastic deposits, and resulted from the increased winnowing of the fine-grained particles by bottom currents.

Acknowledgments

We wish to thank the captain and crew of the RV *Le Suroît* for the quality of the acquired data and Ifremer-Genavir for CARAMBAR cruise organization. We thank the RSMAS of the University of Miami for CARAMBAR 1.5 cruise organization, and the captain and crew of the *Walton Smith* for the quality of the acquired data. This study was supported by the French Institut National des Sciences de l'Univers program "Action Marges" (Contract number: FR00007107). We thank the French Artémis program for radiocarbon measurements. Ludivine Chabaud's PhD project is supported by a grant from TOTAL E&P (Pau, France). We gratefully acknowledge Pascal Lebleu, Olivier Ther, Béatrice Cosson and Bernard Martin for their technical support during the sediment analyses. The authors are grateful to the editor David Van Rooij, the guest editor Andres Rüggeberg and the two anonymous reviewers for their valuable comments which greatly improved this manuscript.

References

Anselmetti, F.S., Eberli, G.P., Ding, Z.-D., 2000. From the Great Bahama Bank into the Straits of Florida: a margin architecture controlled by sea-level fluctuations and ocean currents. GSA Bull. 112, 829–844.
Aurell, M., McNeill, D.F., Guyomard, T., Kindler, P., 1995. Pleistocene shallowing-upward sequences in New Providence, Bahamas; signature of high-frequency sea-level fluctuations in shallow carbonate platforms. J. Sediment. Res. 65, 170–182.
Baringer, M.O.N., Larsen, J.C., 2001. Sixteen years of Florida Current transport at 27° N. Geophys. Res. Lett. 28, 3179–3182.
Bathurst, R.G.C., 1975. Carbonate Sediments and Their Diagenesis. Elsevier, Amsterdam.
Beard, J.H., 1969. Pleistocene paleotemperature record based on planktonic foraminifers, Gulf of Mexico. Trans. Gulf Coast Assoc. Geol. Soc. 26, 185–254.
Beard, J.H., 1973. Pleistocene–Holocene boundary, Wisconsinan substages, Gulf of Mexico. Geol. Soc. Am. Mem. 136, 277–316.

Bergman, K.L., 2005. Seismic Analysis of Paleocurrent Features in the Florida Straits: Insights into the Paleocurrent, Upstream Tectonics, and the Atlantic–Caribbean Connection. University of Miami, p. 190.
Bergman, K.L., Hildegard, W., Janson, X., Poiriez, A.E., G.P., 2010. Controlling parameters on facies geometries of the Bahamas, an isolated carbonate platform environment. In: Westphal, H., Riegl, B., Eberli, G.P. (Eds.), Carbonate Depositional Systems: Assessing Dimensions and Controlling Parameters. Springer, Dordrecht, Heidelberg, London, New York (235 pp.).
Betzler, C., Lüdmann, T., Hübscher, C., Fürstenau, J., 2013. Current and sea-level signals in periplatform ooze (Neogene, Maldives, Indian Ocean). Sediment. Geol. 290, 126–137.
Betzler, C., Lindhorst, S., Eberli, G.P., Lüdmann, T., Möbius, J., Ludwig, J., Schutter, I., Wunsch, M., Reijmer, J.J.G., Hübscher, C., 2014. Periplatform drift: the combined result of contour current and off-bank transport along carbonate platforms. Geology 42, 871–874.
Boardman, M.R., Neumann, A.C., 1984. Sources of periplatform carbonates: Norwest Providence Channel, Bahamas. J. Sediment. Petrol. 54, 1110–1123.
Boardman, M.R., Neumann, A.C., Baker, P.A., Dulin, L.A., Kenter, R.J., Hunter, G.E., Kiefer, K.B., 1986. Banktop responses to Quaternary fluctuations in sea level recorded in periplatform sediments. Geology 14, 28–31.
Bolli, H.M., Saunders, J.B., 1985. Oligocene to Holocene low latitude planktic foraminifera. In: Bolli, H.M., Saunders, J.B., Perch-Nielsen, K. (Eds.), Plankton Stratigraphy. Cambridge University Press, New York, pp. 155–262.
Bosart, L.F., Schwartz, B.E., 1979. Autumnal rainfall climatology of the Bahamas. Mon. Weather Rev. 107, 1663–1672.
Brooks, I.H., Niiler, P.P., 1977. Energetics of the Florida Current. J. Mar. Res. 35, 163–191.
Brunner, C.A., 1975. Evidence for intensified bottom current activity in the Straits of Florida during the last glaciation. Geol. Soc. Am. 7, 1012–1013.
Coplen, T.B., 1988. Normalization of oxygen and hydrogen isotope data. Chem. Geol. (Isot. Geosci. Sect.) 72, 293–297.
Correa, T.B.S., Grasmueck, M., Eberli, G.P., Reed, J.K., Verwer, K., Purkis, S.A.M., 2012. Variability of cold-water coral mounds in a high sediment input and tidal current regime, Straits of Florida. Sedimentology 59, 1278–1304.
Costin, J.M., 1968. Direct current measurements in the Antilles Current. J. Geophys. Res. 73, 3341–3345.
Dill, R.F., Steinen, R.P., 1988. Deposition of Carbonate mud Beds Within High-Energy Subtidal Sand Dunes, Bahamas.
Droxler, A.W., Schlager, W., 1985. Glacial versus interglacial sedimentation rates and turbidite frequency in the Bahamas. Geology 13, 799–802.
Droxler, A.W., Schlager, W., Whallon, C.C., 1983. Quaternary aragonite cycles and oxygen-isotope record in Bahamian carbonate ooze. Geology 11, 235–239.
Ericson, D.B., Ewing, M., Wollin, G., 1964. Pleistocene climates in the Atlantic and Pacific oceans: a comparison based on deep-sea sediments. Science 167, 1483–1485.
Faugères, J.-C., Mulder, T., 2011. Contour currents and contourite drifts. In: Hüneke, H., Mulder, T. (Eds.), Deep-Sea Sediments. Developments in sedimentology, pp. 149–214.
Faugères, J.-C., Stow, D.A.V., 1993. Bottom-current controlled sedimentation: a synthesis of the contourite problem. 82 (1–4), 287–297. Sediment. Geol. 82, 287–297.
Faugères, J.C., Stow, D.A.V., 2008. Contourite drifts. Nature, evolution and controls. In: Rebesco, M., Camerlenghi, A. (Eds.), Developments in Sedimentology, pp. 259–288.
Faugères, J.C., Gonthier, E., Stow, D.A.V., 1984. Contouritic drift molded by deep Mediterranean outflow. Geology 12, 296–300.
Faugères, J.C., Stow, D.A.V., Imbert, P., Viana, A.R., 1999. Seismic features diagnostic of contourite drifts. Mar. Geol. 162, 1–38.
Fernandez-Partegas, J., Mooers, C.N.K., 1975. A synoptic study of winter cold fronts in Florida. Mon. Weather Rev. 103, 742–744.
Gallagher, J.J., 1968. Discussion or paper by J. Michael Costin, 'Direct current measurements in the Antilles Current'. J. Geophys. Res. 73, 7148.
GEBCO, 2014. General Bathymetric Chart of the Oceans. http://www.gebco.net/general_interest/faq/.
Gonthier, E.G., Faugères, J.C., Stow, D.A.V., 1984. Contourite Facies of the Faro Drift, Gulf of Cadiz. Geological Society Special Publication, pp. 275–292.
Grammer, G.M., Ginsburg, R.N., 1992. Highstand versus lowstand deposition on carbonate platform margins: insight from Quaternary foreslopes on the Bahamas. Mar. Geol. 103, 125–136.
Grammer, G.M., Ginsburg, R.N., Harris, P.M., 1993. Timing of deposition, diagenesis, and failure of steep carbonate slopes in response to a high-amplitude/high-frequency fluctuation in sea level, Tongue of the Ocean, Bahamas. In: Loucks, R.G., F.S.J. (Eds.), Carbonate Sequence Stratigraphy: Recent Developments and Applications. AAPG, pp. 107–131.
Gunn, J.T., Watt, D.R., 1982. On the currents and water masses north of the Antilles/Bahamas Arc. J. Mar. Res. 40, 1–48.
Harwood, G.M., Towers, P.A., 1988. Seismic sedimentologic interpretation of a carbonate slope, north margin of Little Bahama Bank. In: Austin, J.A., S.W., et al. (Eds.), Proceeding of the Ocean Drilling Program Scientific result. Ocean Drilling Program, College Station, TX, pp. 263–277.
Heath, K.C., Mullins, H.T., 1984. Open-ocean, off-bank transport of fine-grained carbonate sediment in the Northern Bahamas. Geol. Soc. 15, 199–208.
Hebbeln, D., Wienberg, C., participants, a.c., 2012. Report and preliminary results of R/V Maria S. Merian cruise MSM20-4. WACOM, West Atlantic Cold-Water Coral Ecosystems: the west side story. Berichte, MARUM – Zentrum für Marine Umweltwissenschaften, Fachbereich Geowissenschaften, Universität Bremen, Bridgetown–Freeport, 14 March – 7 April, 2012, p. 120.
Heezen, B.C., Hollister, C.D., 1971. The Face of the Deep. Oxford University Press, London.
Heezen, B.C., Hollister, C.D., Ruddiman, W.F., 1966. Shaping of the continental rise by deep geostrophic bottom currents. Science 152, 502–508.
Hernández-Molina, J., Llave, E., Somoza, L., Fernández-Puga, M.C., Maestro, A., León, R., Medialdea, T., Barnolas, A., García, M., del Río, V.D., Fernández-Salas, L.M., Vázquez, J.T., Lobo, F., Dias, J.M.A., Rodero, J., Gardner, J., 2003. Looking for clues to paleoceanographic imprints: a diagnosis of the Gulf of Cadiz contourite depositional systems. Geology 31, 19–22.
Hickey, B.M., MasCready, P., Elliott, E., Kachel, N.B., 2000. Dense saline plumes in Exuma Sound, Bahamas. J. Geophys. Res. 105, 471–488.
Hine, A.C., Neumann, A.C., 1977. Shallow carbonate-bank–margin growth and structure, Little Bahama Bank, Bahamas. AAPG Bull. 61, 376–406.
Hine, A.C., Wilber, R.J., Bane, J.M., Neumann, A.C., Lorenson, K.R., 1981a. Offbank transport of carbonate sands along open, leeward bank margins: northern Bahamas. Mar. Geol. 42, 327–348.
Hine, A.C., Wilber, R.J., Neumann, A.C., 1981b. Carbonate sand bodies along constrasting shallow bank margins facing open seaways in northern Bahamas. AAPG Bull. 65, 261–290.
Hollister, C.D., Heezen, B.C., 1972. Geological effects of ocean bottom currents: western north Atlantic. In: Gordon, A.L. (Ed.), Studies in Physical Oceanography. Gordon and Breach, New York, pp. 37–66.
Hut, G., 1987. In: Gen., R.t.D. (Ed.), Advisory Group Meeting on Stable Isotope Reference Samples for Geochemical and Hydrological Investigations. Int. At. Energy Agency, Vienna, p. 42 (16–18 September 1985).
Ingham, C., 1974. Velocity and transport of the Antilles current northeast of the Bahama Islands. Fish. Bull. 73, 626–632.
Johns, B., 2011. Cruise report R/V Knorr Cruise KN-200-4. RAPID/MOCHA Program, pp. 1–14.
Kennett, J.P., Huddleston, P., 1972. Late Pleistocene paleoclimatology, foraminiferal biostratigraphy and tephrochronology, western Gulf of Mexico. Quat. Res. 2, 38–69.
Kier, J.S., Pilkey, O., 1971. The influence of sea level changes on sediment carbonate mineralogy, Tongue of the Ocean, Bahamas. Mar. Geol. 11, 189–200.
Knutz, P.C., 2008. Palaeoceanographic significance of contourite drifts. In: Rebesco, M., Camerlenghi, A. (Eds.), Contourites. Developments in Sedimentology, pp. 511–535.
Lantzsch, H., Roth, S., Reijmer, J.J.G., Kinkel, H., 2007. Sea-level related resedimentation processes on the northern slope of Little Bahama Bank (Middle Pleistocene to Holocene). Sedimentology 54, 1307–1322.
Lee, T.N., Johns, W., Schott, F., Zantopp, R., 1990. Western boundary current structure and variability east of Abaco, Bahamas at 26.5° N. J. Phys. Oceanogr. 20, 446–466.
Lee, T.N., Johns, W.E., Zantopp, R., 1996. Moored observations of western boundary current variability and thermohaline circulation 26.5° N in the subtropical north Atlantic. J. Phys. Oceanogr. 26, 962–963.
Lisiecki, L.E., Raymo, M.E., 2005. A Pliocene–Pleistocene stack of 57 globally distributed benthic d18O records. Paleoceanography 20.
Llave, E., Schönfeld, J., Hernández-Molina, F.J., Mulder, T., Somoza, L., Díaz del Río, V., Sánchez-Almazo, I., 2006. High-resolution stratigraphy of the Mediterranean outflow contourite system in the Gulf of Cadiz during the late Pleistocene: the impact of Heinrich events. Mar. Geol. 227, 241–262.
Lynts, G.W., Judd, J.B., Stehman, C.F., 1973. Late Pleistocene history of Tongue of the Ocean, Bahamas. Geol. Soc. Am. Bull. 84, 2665–2684.
Malone, M.J., Slowey, N.C., Henderson, G.M., 2001. Early diagenesis of shallow-water periplatform carbonate sediments, leeward margin, Great Bahama Bank (ocean drilling program leg 166). GSA Bull. 113, 881–894.
Martin, R.E., Johnson, G.W., Neff, E.D., Krantz, D.W., 1990. Quaternary planktonic foraminiferal assemblage zones of the northeast Gulf of Mexico, Colombia basin (Caribbean Sea), and tropical Atlantic Ocean: graphic correlation of microfossil and oxygen isotope datums. Paleoceanography 5, 531–555.
Masaferro, J.L., Eberli, G.P., 1999. Jurassic–Cenozoic structural evolution of the southern Great Bahama Bank. In: Mann, P. (Ed.), Caribbean Basins: Sedimentary Basins of the World, pp. 167–193.
McNeill, D.F., Grammer, G.M., Williams, S.C., 1998. A 5 MY chronology of carbonate platform margin aggradation, southwestern Little Bahama Bank, Bahamas. J. Sediment. Res. 68, 603–614.
Messing, C.G., Neumann, A.C., Lang, J.C., 1990. Biozonation of deep-water lithoherms and associated hardgrounds in the northeastern Straits of Florida. PALAIOS 5, 15–33.
Migeon, S., Weber, O., Faugères, J.-C., Saint-Paul, J., 1999. SCOPIX: a new X-ray imaging system for core analysis. Geo-Mar. Lett. 18, 251–255.
Miller, K.G., Mountain, G.S., Wright, J.D., B.J., V., 2011. A 180-million-year record of sea level and ice volume variations from continental margin and deep-sea isotopic records. Oceanography 24, 40–53.
Morse, J.W., Mackenzie, F.T., 1990. Geochemitry of sedimentary carbonates. Dev. Sedimentol.
Mulder, T., Ducassou, E., Eberli, G.P., Hanquiez, V., Gonthier, E., Kindler, P., Principaud, M., Fournier, F., Léonide, P., Billeaud, I., Marsset, B., Reijmer, J.J.G., Bondu, C., Joussiaume, R., Pakiades, M., 2012a. New insights into the morphology and sedimentary processes along the western slope of Great Bahama Bank. Geology 40, 603–606.
Mulder, T., Ducassou, E., Gillet, H., Hanquiez, V., Tournadour, E., Combes, J., Eberli, G.P., Kindler, P., Gonthier, E., Conesa, G., Robin, C., Sianipar, R., Reijmer, J.J.G., François, A., 2012b. Canyon morphology on a modern carbonate slope of the Bahamas: evidence of a regional tectonic tilting. Geology 40, 771–774.
Mulder, T., Hassan, R., Ducassou, E., Zaragosi, S., Gonthier, E., Hanquiez, V., Marchès, E., Toucanne, S., 2013. Contourites in the Gulf of Cadiz: a cautionary note on potentially ambiguous indicators of bottom current velocity. Geo-Mar. Lett. 33, 357–367.
Mullins, H.T., 1983. Comments and reply on 'Eustatic control of turbidites and winnowed turbidites'. Geology 11, 57–60.
Mullins, H.T., Neumann, A.C., 1979. Deep carbonate bankmargin structure and sedimentation in the northern Bahamas. SEPM Spec. Publ. 7, 165–192.
Mullins, H.T., Neumann, A.C., Wilber, R.J., Hine, A.C., Chinburg, S.J., 1980. Carbonate sediment drifts in northern Straits of Florida. Am. Assoc. Pet. Geol. Bull. 64, 1701–1717.
Mullins, H.T., Newton, C.R., Heath, K., Vanburen, H.M., 1981. Modern deep-water coral mounds north of Little Bahama Bank: criteria for recognition of deep-water coral bioherms in the rock record. J. Sedim. Petrol. 51, 999–1013.

Mullins, H.T., Heath, K.C., Van Buren, H.M., Newton, C.R., 1984. Anatomy of a modern open-ocean carbonate slope: northern Little Bahama Bank. Sedimentology 31, 141–168.
Mullins, H.T., Wise, S.W.J., Gardulski, A.F., Hinchey, E.J., Masters, P.M., Siegel, D.I., 1985. Shallow subsurface diagenesis of Pleistocene periplatform ooze: northern Bahamas. Sedimentology 32, 473–494.
Murdmaa, I., Borisov, D., Ivanova, E., Levchenko, O., Emelyanov, E., Dorokhova, E., Dara, O., Sivkov, V., 2015. The Ioffe calcareous contourite drift, western south Atlantic. Mar. Geol. (in this issue).
Neumann, A.C., Ball, M.M., 1970. Submersible observations in the Straits of Florida: geology and bottom currents. Geol. Soc. Am. Bull. 81, 2861–2874.
Neumann, A.C., Land, L., 1975. Lime mud deposition and calcareous algae in the bight of Abaco, Bahamas: a budget. J. Sediment. Petrol. 45, 763–786.
Neumann, G., Pierson, W.J., 1966. Principles of Physical Oceanography. Prentice-Hall, Inc., Englewood Cliffs, N.J.
Neumann, A.C., Kofoed, J.W., Keller, G.H., 1977. Lithoherms on the Straits of Florida. Geology 5, 4–10.
Pilskaln, C.H., Neumann, A.C., Bane, J.M., 1989. Periplatform carbonate flux in the northern Bahamas. Deep-Sea Res. 36, 1391–1406.
Poag, C.W., Valentine, P.C., 1976. Biostratigraphy and ecostratigraphy of the Pleistocene basin, Texas–Louisiana continental shelf. Trans. Gulf Coast Assoc. Geol. Soc. 26, 185–254.
Rankey, E.C., Doolittle, F., 2012. Geomorphology of carbonate platform-marginal uppermost slopes: insights from a Holocene analogue, Little Bahama Bank, Bahamas. Sedimentology 59, 2146–2171.
Rebesco, M., Camerlenghi, A., 2008. Contourites. Elsevier.
Rebesco, M., Wåhlin, A., Laberg, J.S., Schauer, U., Beszczynska-Möller, A., Lucchi, R.G., Noormets, R., Accettella, D., Zarayskaya, Y., Diviacco, P., 2013. Quaternary contourite drifts of the Western Spitsbergen margin. Deep-Sea Res. I Oceanogr. Res. Pap. 79, 156–168.
Rebesco, M., Hernández-Molina, F.J., Van Rooij, D., Wåhlin, A., 2014. Contourites and associated sediments controlled by deep-water circulation processes: state-of-the-art and future considerations. Mar. Geol. 352, 111–154.
Reed, J.K., 2002. Comparison of deep-water coral reefs and lithoherms off southeastern USA. Hydrobiologia 471, 57–69.
Reijmer, J.J.G., Schlager, W., Droxler, A.W., 1988. Site 632: Pliocene–Pleistocene sedimentation in a Bahamian Basin. In: Austin, J.A., Schlager, W., Palmer, A. (Eds.), Proceedings Ocean Drilling Program, Scientific Results. Ocean Drilling Program, College Station, pp. 213–220.
Rendle, R.H., Reijmer, J.J.G., Kroon, D., Henderson, G.M., 2000. Mineralogy and sedimentology of the Pleistocene to Holocene on the Leeward margin of Great Bahama Bank. In: Swart, P.K., Eberli, G.P., Malone, M.J., Sarg, J.F. (Eds.), Proc. ODP, Sci. Results, 166. College Station, TX (Ocean Drilling Program), pp. 61–76.
Rendle, R., Reijmer, J.J.G., 2002. Quaternary slope development of the western leeward margin of the Great Bahama Bank. Mar. Geol. 185, 143–164.
Rendle-Bühring, R.H., Reijmer, J.J.G., 2005. Controls on grain-size patterns in periplatform carbonates: marginal setting versus glacio-eustacy. Sediment. Geol. 175, 99–113.
Roberts, H.H., Rouse, L.J., Walker, N.D., Hudson, J.H., 1982. Cold-water stress in Florida Bay and northern Bahamas: a product of winter cold-air outbreaks. J. Sediment. Petrol. 52, 145–155.
Roth, S., Reijmer, J.J.G., 2004. Holocene Atlantic climate variations deduced from carbonate periplatform sediments (leeward margin, Great Bahama Bank). Paleoceanography 19, PA1003.
Roth, S., Reijmer, J.J.G., 2005. Holocene millennial to centennial carbonate cyclicity recorded in slope sediments of the Great Bahama Bank and its climatic implications. Sedimentology 52, 161–181.
Rousset, C., Beal, L.M., 2014. Closing the transport budget of the Florida Straits. Geophys. Res. Lett. 41, 1–7.
Rowe, E., Mariano, A.J., Ryan, E.H., 2015. "The Antilles Current" ocean surface currents World wide web article, accessed April 2005. Available online at: http://oceancurrents.rsmas.miami.edu/atlantic/antilles.html.
Ruddiman, W.F., 1971. Pleistocene sedimentation in the equatorial Atlantic: stratigraphy and faunal paleoclimatology. Geol. Soc. Am. Bull. 82, 283–302.
Sato, T., Kameo, K., Takayama, T., 1991. Coccolith biostratigraphy of the Arabian Sea. In: Prell, W.L., Niitsuma, N. (Eds.), Proceeding ODP, Sciences Results. Ocean Drilling Program, College Station, TX, pp. 37–54.
Schlager, W., James, N.P., 1978. Low-magnesian calcite limestones forming at the deep-sea floor, Tongue of the Ocean, Bahamas. Sedimentology 25, 675–702.
Schlager, W., Reijmer, J.J.G., Droxler, A.W., 1994. Highstand shedding of carbonate platforms. J. Sediment. Res. B64, 270–281.
Sealey, N.E., 1994. Bahamian Landscapes: An Introduction to the Geography of the Bahamas. Media Publishing, Nassau, Bahamas.
Sheridan, R.E., Drake, C.L., Nafe, J.E., Hennion, J., 1966. Seismic-refraction study of continental margin east of Florida. Bull. Am. Assoc. Pet. Geol. 50, 1972–1991.
Shinn, E.A., Steinen, R.P., Lidz, B., Swart, P.K., 1989. Whitings, a sedimentologic dilemma. J. Sedim. Petrol. 59, 147–161.
Shinn, E.A., Steinen, R.P., Dill, R.F., Major, R., 1993. Lime-mud layers in high-energy tidal channels: a record of hurricane deposition. Geology 21, 603–606.
Siddall, M., Rohling, E.J., Almongi-Labin, A., Hemleben, C., Meischner, D., Schmeizer, I., Smeed, D.A., 2003. Sea-level fluctuations during the last glacial cycle. Nature 423, 853–858.
Stow, D.A.V., Holbrook, J.A., 1984. North Atlantic contourites: an overview. Geol. Soc. Lond., Spec. Publ. 15, 245–256.
Stow, D.A.V., Pudsey, C.J., Howe, J.A., Faugères, J.-C., Viana, A.R., 2002. Deep-water contourite systems: modern drifts and ancient series, seismic and sedimentary characteristics. Geol. Soc. Lond. Mem. 22, 464.
Stow, D.A.V., Hunter, S., Wilkinson, D., Hernández-Molina, F.J., 2008. The nature of contourite deposition. In: Rebesco, M., Camerlenghi, A. (Eds.), Contourites. Developments in Sedimentology, pp. 143–156.
Swart, P.K., Oehlert, A.M., Mackenzie, G.J., Eberli, G.P., Reijmer, J.J.G., 2014. The fertilization of the Bahamas by Saharan dust: a trigger for carbonate precipitation? Geology 42, 671–674.
Thierstein, H.R., Geitzenauer, K.R., Molfino, B., Shackleton, N.J., 1977. Global synchroneity of late Quaternary coccolith datum levels : validation by oxygen isotopes. Geology 400-404.
Toucanne, S., Jouet, G., Ducassou, E., Bassetti, M.-A., Dennielou, B., Angue Minto'o, C.M., Lahmi, M., Touyet, N., Charlier, K., Lericolais, G., Mulder, T., 2012. A 130,000-year record of Levantine intermediate water flow variability in the Corsica Trough, western Mediterranean Sea. Quat. Sci. Rev. 33, 55–73.
Tournadour, E., 2015. Architecure et Dynamique Sédimentaire d'une Pente Carbontée Moderne: Exemple de la Pente Nord de Little Bahama Bank (LBB), Bahamas. Université de Bordeaux, Pessac, p. 282.
Tournadour, E., Mulder, T., Borgomano, J., Hanquiez, V., Ducassou, E., Gillet, H., 2015. Origin and architecture of a mass transport complex on the northwest slope of Little Bahama Bank (Bahamas): relations between off-bank transport, bottom current sedimentation and submarine landslides. Sediment. Geol. 317, 9–26.
Traverse, A., Ginsburg, R.N., 1966. Palynology of the surface sediments of Great Bahama Bank, as related to water movement and sedimentation. Mar. Geol. 4, 417–459.
Van Rooij, D., Iglesias, J., Hernández-Molina, F.J., Ercilla, G., Gomez-Ballesteros, M., Casas, D., Llave, E., De Hauwere, A., Garcia-Gil, S., Acosta, J., Henriet, J.P., 2010. The Le Danois contourite depositional system: interactions between the Mediterranean outflow water and the upper Cantabrian slope (North Iberian margin). Mar. Geol. 274, 1–20.
Vandorpe, T., Van Rooij, D., Stow, D.V., Henriet, J.-P., 2011. Pliocene to recent shallow-water contourite deposits on the shelf and shelf edge off south-western Mallorca, Spain. Geo-Mar. Lett. 31, 391–403.
Vandorpe, T., Van Rooij, D., de Haas, H., 2014. Stratigraphy and paleoceanography of a topography-controlled contourite drift in the Pen Duick area, southern Gulf of Cádiz. Mar. Geol. 349, 136–151.
Veizer, J., 1983. Trace elements and isotopes in sedimentary carbonates. In: Reefer, R.J. (Ed.), Carbonates: Mineralogy and Chemistry. Mineralogical Society of America, Reviews in Mineralogy, Washington, DC, pp. 265–299.
Voelker, A.H.L., Lebreiro, S.M., Schönfeld, J., Cacho, I., Erlenkeuser, H., Abrantes, F., 2006. Mediterranean outflow strengthening during northern hemisphere coolings: a salt source for the glacial Atlantic? Earth Planet. Sci. Lett. 245, 39–55.
Wefer, G., Berger, W.H., Richter, C., 1998. Ch 2. Explanatory notes — shipboard scientific party. Proceedings of the Ocean Drilling Program, Initial Reports. 175.
Wilber, R.J., 1976. Petrology of Submarine-Lithified Hardgrounds ans Lithoherms from the Deep Flank Environnement of Little Bahama Bank (Northeastern Straits of Florida). Duke University, Durham, p. 241.
Wilber, R.J., Milliman, J.D., Halley, R.B., 1990. Accumulation of bank-top sediment on the western slope of Great Bahama Bank: rapid progradation of a carbonate megabank. Geology 18, 970–974.
Williams, S.C., 1985. Stratigraphy, Facies Evolution and Diagenesis of Late Cenozoic Limestones and Dolomites, Little Bahama Bank, Bahamas. Univ. Miami, Coral Gables FL (217 pp.).
Wilson, B., 2012. Percentage carrying capacity in fossil successions: a new ecostratigraphic tool with potential for detecting palaeoenvironmental change illustrated using bathyal benthic foraminifera in the Late Quaternary of ODP hole 1006A, Santaren Channel. Palaeogeogr. Palaeoclimatol. Palaeoecol. 337–338, 143–150.
Wilson, B., 2013. Ecostratigraphic regime shift during late Quaternary marine isotope stages 8–9 in Santaren channel, western tropical Atlantic Ocean: benthonic foraminiferal evidence from ODP hole 1006A. J. Foraminifer. Res. 43, 143–153.
Wilson, P.A., Roberts, H.H., 1992. Carbonate-periplatform sedimentation by density flows: a mechanism for rapid off-bank and vertical transport of shallow-water fines. Geology 20, 713–716.
Wilson, P.A., Roberts, H.H., 1995. Density cascading: off-shelf sediment transport, evidence and implications, Bahama Banks. J. Sediment. Res. A65, 45–56.
Zaragosi, S., Bourillet, J.-F., Eynaud, F., Toucanne, S., Denhard, B., Van Toer, A., Lanfumey, V., 2006. The impact of the last European deglaciation on the deep-sea turbidite systems of the Celtic-Armorican margin (Bay of Biscay). Geo-Mar. Lett. 26, 317–329.